

Excited-State Absorption: Reference Oscillator Strengths, Wave Function, and TDDFT Benchmarks

Jakub Širůček, Boris Le Guennic,* Yann Damour, Pierre-François Loos,* and Denis Jacquemin*



Cite This: *J. Chem. Theory Comput.* 2025, 21, 4688–4703



Read Online

ACCESS |

Metrics & More

Article Recommendations

Supporting Information

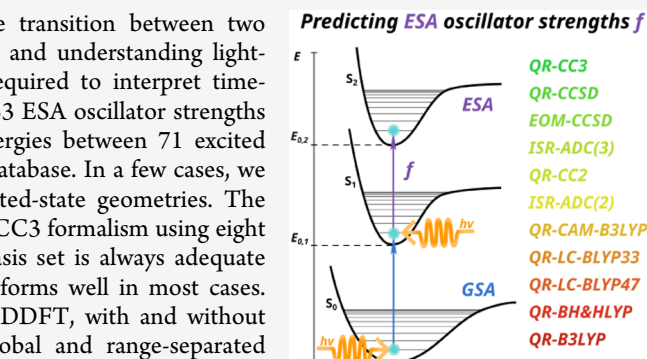
ABSTRACT: Excited-state absorption (ESA) corresponds to the transition between two electronic excited states and is a fundamental process for probing and understanding light-matter interactions. Accurate modeling of ESA is indeed often required to interpret time-resolved experiments. In this contribution, we present a dataset of 53 ESA oscillator strengths in three different gauges and the associated vertical transition energies between 71 excited states of 21 small- and medium-sized molecules from the QUEST database. In a few cases, we additionally investigated the effect of geometry relaxation on excited-state geometries. The reference values were obtained within the quadratic response (QR) CC3 formalism using eight different Dunning basis sets. We found that the d-aug-cc-pVTZ basis set is always adequate while its more compact double- ζ counterpart, d-aug-cc-pVQZ, performs well in most cases. These QR-CC3 data allow us to assess the performance of QR-TDDFT, with and without applying the Tamm-Dancoff approximation, using a panel of global and range-separated hybrids (B3LYP, BH&HLYP, CAM-B3LYP, LC-BLYP33, and LC-BLYP47), as well as several lower-order wave function methods, i.e., QR-CCSD, QR-CC2, EOM-CCSD, ISR-ADC(2), and ISR-ADC(3). We show that QR-TDDFT delivers acceptable errors for ESA oscillator strengths with CAM-B3LYP showing particular promise, especially for the largest molecules of our set, and in the Franck–Condon (FC) region. We also find that ISR-ADC(3) exhibits excellent performance in this region. When using excited-state optimal geometries, the relative performance of wave function-based approaches remains consistent with trends observed in the Franck–Condon region. However, for TD(A)-DFT, the accuracy varies significantly, as the performance of different exchange-correlation functionals significantly depends on the chosen geometry.

1. INTRODUCTION

During a typical ground-state absorption (GSA), the electronic cloud is excited from its ground state to an excited state (ES) by absorbing a photon. Excited-state absorption (ESA) is a similar process wherein the electronic transition occurs between two ESs. In transient spectroscopies, ESA stands as a crucial photophysical phenomenon for probing and understanding light-matter interactions.¹

ESA is key to a wide range of technological applications from solar cells,² lasers,³ and light-emitting diodes,⁴ to chemical sensors,⁵ optical amplifiers,⁶ and optical power-limiting devices.^{7–9} In these applications, transitions between ESs play a pivotal role in device operation and are parts of the many complex ES processes occurring in, e.g., exciton-exciton annihilation,¹⁰ exciton-polaron quenching,¹¹ electric-field-induced ionization of excitons,¹² reabsorption of emitted light by polarons,¹³ and two-photon absorption.^{8,9}

Illustratively, combining ESA with two-photon absorption in optical power-limiting devices allows for maintaining transparency at low light intensities while achieving increased absorption at higher intensities, paving the way to eye-protecting devices. This approach has been demonstrated in several molecular architectures such as organic and organometallic cyanines⁸ and twistacenes.⁹



Accurate reference ESA data are thus increasingly sought after for their relevance in designing improved molecules and materials. Moreover, in many experiments, ESA cannot be easily separated from other photoinduced signatures contributing to the spectral properties in the same energy range, and thus accurate calculations of ESA are helpful to distinguish ESA from other phenomena.^{13–15}

When computing ESA properties, two aspects ought to be considered: the energy difference, often expressed as the difference of vertical excitation energies ($\Delta E_{m,n}$) between the m th and n th ESs, and the transition probability, which can be expressed in terms of transition dipole moments (μ) or oscillator strengths (f), these properties being typically more demanding to determine than the energies.

To obtain f values for ESA, or GSA, one has to select an appropriate electronic structure method. Among the most widely used ones for ESA are various flavors of coupled-cluster

Received: January 28, 2025

Revised: April 2, 2025

Accepted: April 3, 2025

Published: April 14, 2025



(CC) theory, such as CC2,^{16–18} and CCSD,^{17–22} multi-reference (MR) approaches, most notably CASPT2 (second-order complete-active-space perturbation theory),^{18,23,24} and, of course, time-dependent density-functional theory (TDDFT).^{21–23,25–32} The latter is computationally cheap and remains the most widely employed in practice. However, TDDFT results significantly depend on the selected exchange-correlation functional (XCF), often leading to unanswered questions regarding the accuracy that can be expected from TDDFT.

CC3^{17,18,21,22} is an iterative CC formalism that includes single, double, and triple excitations.³³ It has been shown to deliver highly accurate ES estimates with, in particular, $\Delta E_{0,n}$ ($m = 0$ being the GS) and GSA oscillator strengths that can serve as solid references for benchmark studies.^{34–36} Hence, we rely on CC3 to establish our reference ESA values in the present work.

More globally, CC approaches are, in general, more user-friendly than MR methods as it requires virtually no knowledge about the system and its corresponding ESs. It is thus a preferable choice when dealing with ESs possessing a dominant single-reference (SR) character in a low-coupling region.¹⁸ Additionally, the accuracy of CC-based f values can be probed by gauge invariance.^{37,38} Indeed, the oscillator strengths can be computed in the length, velocity, and mixed gauges, as follows

$$f_{m,n}^l = \frac{2\Delta E_{m,n}}{3} \langle m|\mathbf{r}|n\rangle \langle n|\mathbf{r}|m\rangle \quad (1a)$$

$$f_{m,n}^v = \frac{2}{3\Delta E_{m,n}} \langle m|\mathbf{p}|n\rangle \langle n|\mathbf{p}|m\rangle \quad (1b)$$

$$f_{m,n}^m = -\frac{2i}{3} \langle m|\mathbf{r}|n\rangle \langle n|\mathbf{p}|m\rangle \quad (1c)$$

where f with superscripts l, v, and m denote the oscillator strengths in length, velocity, and mixed gauge, respectively, of the transition between the m th and n th ESs, \mathbf{r} is the length operator and \mathbf{p} the momentum operator. As a reminder, we denote the GSA vertical excitation energy as $\Delta E_{0,n}$ and the corresponding ESA energy as $\Delta E_{m,n}$. For the exact wave function, that is, the full configuration interaction (FCI) wave function computed in a complete basis set, these three equations deliver the same results, illustrating the expected gauge invariance for the exact wave function.³⁹ Hence, when one considers an approximate level of theory, inspecting the difference between the three gauges is a crude metric of the accuracy of the calculated f values. Indeed, it was shown by Pawłowski et al.,³⁷ using the CCS, CC2, CCSD, and CC3 series, and later by some of us,³⁴ that the difference between GSA oscillator strengths obtained in different gauges becomes markedly smaller when the maximum excitation degree of the cluster operator increases. Of course, when the desired ESs exhibit MR characters, SR approaches become less efficient and one has to rely on MR schemes such as the popular CASPT2 formalism.²³ MR methods can, in principle, accurately describe all ESs but can be challenging to use.^{18,23,40}

At this stage, we recall that there are two main CC approaches for computing ES properties: the equation-of-motion (EOM)⁴¹ and response function formalisms, the latter being also known as response theory (RT).^{19,39} In the RT approach, time-independent expectation values of molecular properties are expanded in orders of a frequency-dependent perturbation leading to results equivalent to those reached with

numerical derivatives. In the EOM formalism, molecular properties are computed directly from the expectation value of the corresponding operator for the physical observable. It should be noted that both approaches yield the same vertical excitation energies but differ in transition dipoles. Nevertheless, at high levels of theory, such as CC3, the computationally less expensive EOM gives GSA f values very similar to the ones obtained with RT.^{34,42–45}

Apart from RT and EOM, we wish to mention the intermediate state representation (ISR) which has been extensively used within the ADC (algebraic diagrammatic construction) family of methods, e.g., ADC(2) and ADC(3).^{46,47} In this work, we primarily focus on the RT approach, which has been widely used for GSA and, in several cases, for ESA calculations as well, and is readily applicable within TDDFT.^{18,23,25,28,29}

In the RT framework, there are, in principle, two options for obtaining the ESA f values: from the single residues of the linear response (LR) function of one of the two ESs involved in the ESA or from the double residues of the quadratic response (QR) function of the ground state.^{9,18} The latter formalism allows not only calculating the ESA oscillator strengths but also two-photon absorption properties which are often sought after in combination with ESA,^{8,9} as discussed above.

To the best of our knowledge, the first seminal study testing different RT approaches for ESA calculations was performed by Norman et al.⁴⁸ Both SR and MR models were tested with cubic and linear RTs on the ESs of benzene and naphthalene. With cubic response theory, one can obtain ES polarizabilities in a similar fashion as computing f values with QR. For the ES polarizabilities, the authors found a good performance of the cubic response theory, which in some cases outperformed the LR approach.

Subsequent studies by Cronstrand et al. in 2000¹⁸ and 2001¹⁷ further explored ESA with different methods. In the former work, the authors compared the QR and LR with a hierarchy of CC methods [CCS, CC2, CCSD, CCSDR(3), and CC3] on small molecules, confirming the superiority of the QR approach. In the second study, the QR approach was tested with the same hierarchy of CC methods on butadiene and a set of polyenes. Both works showed a very good agreement between CC3 f and $\Delta E_{0,n}$ values and the corresponding experimental data when a triple- ζ basis set is employed. Moreover, a systematic convergence of μ in the CC series was reported.

We underline that in the case of CC3 and CCSDR(3), both studies computed the f values using CCSD μ values and the corresponding CC3 or CCSDR(3) energies. This approach was necessary because, on the one hand, CCSDR(3) does not allow for calculating μ values within the RT formalism, owing to its noniterative treatment of triple excitations,⁴⁹ while, on the other hand, CC3 theoretically permits such calculations, albeit no implementation was available at the time.

Of course, most wave function approaches are computationally expensive, which poses a significant limitation, especially in ESA applications where the molecules of interest are typically organic or organometallic dyes, sometimes with an oligomeric or polymeric character.^{2–8} For these reasons, QR-TDDFT is a cheap and useful alternative to wave function approaches.

The first work, to the best of our knowledge, utilizing QR-TDDFT for ESA calculations, was published by Ling et al. in

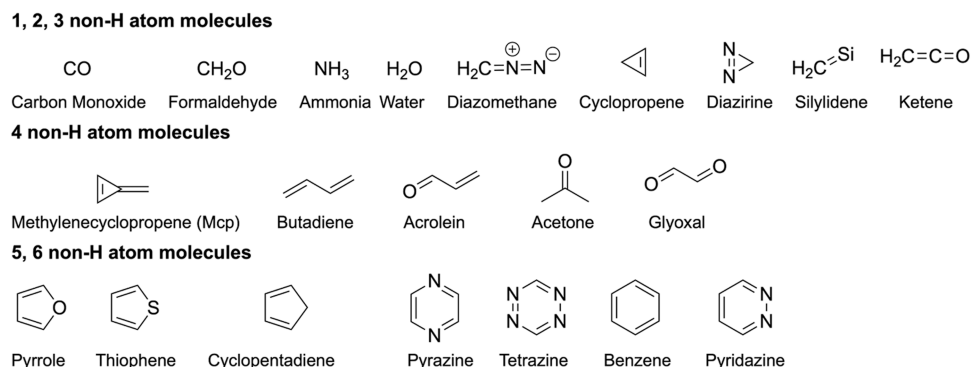


Figure 1. Schematic representation of the molecules considered in this study.

2013.²⁸ In this study, QR-TDDFT was applied to model near-infrared (NIR) spectra of oligofluorenes, molecules that are considerably larger than those typically accessible by wave function-based methods. The authors demonstrated a good qualitative agreement with the measured ESA spectra corresponding to transitions from the S_1 state. Subsequently, the performance of QR-TDDFT was compared with its linear counterpart using the same set of oligofluorenes.²⁹ While the computationally cheaper LR model^{26,31,50} provided energies similar to those obtained with QR in the NIR region, significant variations were observed for the f values. Both studies were limited to a dataset of 7 oligofluorenes and mainly focused on transitions from the S_1 state. A wider set of fluorene homo- and copolymers was investigated by Denis et al. in 2016⁵¹ within the Tamm–Dancoff approximation (TDA) of QR-TDDFT. Their findings also showed good qualitative agreement with the experimental data in the NIR region. We underline that these studies revealed minimal sensitivity of the ESA spectra to geometry relaxation from the Franck–Condon geometry to the S_1 minima. Following these initial investigations, the amount of ESA QR-TDDFT calculations has grown over the past few years.^{21,22,25,27,32} While consistent qualitative agreement has been achieved for energetically low-lying ESA transitions,^{30,52} challenges persist for higher-lying transitions.⁵³ One of the significant obstacles for capturing the higher-lying ESA transitions is state characterization, as pinpointed by Roldao et al.²³

Despite the availability of benchmarks and datasets for GSA, such as the QUEST,⁵⁴ VERDE,⁵⁵ and QM-symex²⁸ databases, reference ESA data remain scarce. A comprehensive benchmark covering a wide range of f values, different methods, XCFs (for TDDFT), and basis sets for ESA is lacking. Here, we present such a database comprising 53 ES transitions in 21 molecules containing from 1 to 6 (non-hydrogen) atoms. The selected transitions occur between energetically low-lying Rydberg and valence ESs with a predominant single excitation character.

Below, we first investigate the convergence of f values at the QR-CC3 level to establish computationally attainable yet trustworthy reference values. For this purpose, we compute the values of the oscillator strengths in all three gauges (length, velocity, and mixed) with eight different correlation-consistent basis sets varying in the level of augmentation with diffuse functions (single to triple) and ζ -multiplicity (double to quadruple) on a set of small molecules. To further confirm our choice of a reference level of theory, we carry out extrapolated FCI calculations. Next, we conduct the remaining part of the QR-CC calculations in four basis sets, which we also employ to

assess the ISR implementation of the second-order ADC [ISR-ADC(2)],⁴⁷ which was shown to yield results of accuracy similar to CC2 for GSA.^{34,35} For the rest of our study, we utilize the selected reference d-aug-cc-pVTZ basis set only and evaluate various wave function approaches [ISR-ADC(3) and EOM-CCSD] as well as QR-DTDFT, with and without TDA. We choose two global hybrids, B3LYP,^{56–59} BH&HLYP,⁶⁰ and three range-separated hybrids, namely, CAM-B3LYP,⁶¹ and two different versions of LC-BLYP.⁶² The two versions vary in the range separation parameter ω and we refer to them as LC-BLYP33 ($\omega = 0.33 \text{ bohr}^{-1}$) and LC-BLYP47 ($\omega = 0.47 \text{ bohr}^{-1}$).

Lastly, to assess whether the trends obtained on S_0 geometries remain valid on excited-state structures, we use optimal S_1 and S_2 structures and perform a benchmark of all methods, using the dAVTZ basis, for f and $\Delta E_{m,n}$ on a subset of 4 molecules and 14 transitions.

We anticipate that the comprehensive dataset generated in this study will be helpful in the field of ESA calculations and will hopefully contribute to the design and development of novel functional materials.

2. COMPUTATIONAL DETAILS

The selected set of 21 molecules is shown in Figure 1. All calculations performed in the Franck–Condon region were done using the CC3/AVTZ ground-state geometries of the QUEST database.⁵⁴ The optimal ES geometries were obtained at different levels of theory as reported in the Supporting Information (SI) and were previously optimized by some of us.⁶³ Cartesian coordinates are provided in the SI. Our computations employ the frozen-core approximation, except for the TD(A)-DFT calculations. Unless otherwise noted, the default convergence thresholds and algorithms of the selected codes were used.

All QR-CC calculations (CC2, CCSD, and CC3) of f values in all three gauges were done using the double residues of the quadratic response function within the approach implemented in Dalton 2020.^{64–67} All QR-CC f values were taken directly from the Dalton output except for the mixed gauge. While computing f in the mixed gauge, Dalton often prints the correct absolute value of f but with a negative sign. We suspect that this is a misprint. When the value of f is recomputed from the transition strengths, printed in the Dalton output, as expressed in eq 1c, it indeed yields the same absolute value with the correct (positive) sign. Therefore, in such cases, we only report the absolute f values.

QR-CC calculations were first conducted on a small set of transitions in compact molecules: ammonia, carbon monoxide,

diazirine, silylidene, and water with a total of eight Dunning augmented correlation-consistent basis sets, as implemented in Dalton: *aug-cc-pVDZ* (AVDZ), *d-aug-cc-pVDZ* (dAVDZ), *aug-cc-pVTZ* (tAVDZ), *aug-cc-pVTZ* (AVTZ), *d-aug-cc-pVTZ* (dAVTZ), *t-aug-cc-pVTZ* (tAVTZ), *aug-cc-pVQZ* (AVQZ), *d-aug-cc-pVQZ* (dAVQZ). The dAVTZ basis set was deemed sufficiently complete for our purposes with an acceptable computational cost and was thus employed to establish our reference values (*vide infra*). After this preliminary examination, the rest of the QR-CC and ADC(2) calculations were performed with the AVDZ, dAVDZ, AVTZ, and dAVTZ basis sets only.

All ESA ADC(2) and ADC(3) values were obtained using ISR as implemented in Q-Chem 6.0.^{68,69} The SCF convergence threshold was set to at least 10^{-8} a.u. When the requested ESs did not converge, the default number of iterations in the Davidson procedure was increased. The same four basis sets as above were used for ADC(2), each combined with the appropriate auxiliary basis, as defined in Q-Chem. On top of that, a smaller secondary basis set (cc-pVTZ) was used for the initial guess at the beginning of all AVTZ and dAVTZ calculations. In the case of ADC(3), we used only the dAVTZ basis set. In a few cases, when the target molecule possesses high symmetry, the program could not determine the irreducible representations of the orbitals. In such cases, the calculations were performed without the secondary initial guess basis set. Only length gauge f values were obtained with ADC.

All EOM-CCSD calculations were done using Q-Chem 6.0.⁴¹ We ensured the correct state assignment by comparison with Dalton's QR-CCSD vertical excitation energies $\Delta E_{0,n}$ maintaining an acceptable numerical error of 0.01 eV. The calculated f values were verified to correspond to transitions from the lower-energy ES to the higher-energy one. The dAVTZ basis set was considered. Similar to the ADC(2) and ADC(3) calculations, the appropriate auxiliary basis set was used alongside a smaller secondary basis set. However, the latter was occasionally omitted when molecular symmetry constraints prevented its application. Only length gauge f values were obtained with EOM-CCSD.

We tested five different XCJs: two global hybrids, namely B3LYP^{56–59} (20% of exact exchange), and BH&HLYP⁶⁰ (50% of exact exchange), and three range-separated hybrids, namely CAM-B3LYP,⁶¹ with exact exchange ranging from 19% to 65% and a range separation parameter ω of 0.33 bohr⁻¹, and two different versions of LC-BLYP⁶² for which exact exchange ranges from 0 to 100%. The two versions vary in the range separation parameter ω and we refer to them as LC-BLYP33 ($\omega = 0.33$ bohr⁻¹) and LC-BLYP47 ($\omega = 0.47$ bohr⁻¹). All ESA TDDFT calculations, with and without TDA, of $\Delta E_{m,n}$ and f , in length gauge, were done using the double residues of the quadratic response function as implemented in Dalton 2020.^{70–72} Only the dAVTZ basis set was used as implemented in Dalton. A SCF convergence threshold of at least 10^{-8} a.u. was used. The transition dipoles in the length and velocity gauges were obtained as the norm of the corresponding x , y , and z transition dipole moments printed in the Dalton output. The final f values were then computed according to eqs 1a and 1b.

Extrapolated FCI values were derived from CIPSI calculations performed using the quantum package software.⁷³ For each transition, the two states of interest were identified based on EOM-CCSD results and extracted from the CIS wave

function. CIPSI calculations were carried out for each pair of states using the state-following procedure employed in ref 74. The extrapolated FCI values and associated uncertainties were then obtained through a 4-point weighted quadratic fit, following the procedure explained in ref 74. Since two states were involved, the extrapolations rely on the average of their respective second-order energies, as detailed in ref 75.

3. RESULTS AND DISCUSSION

To analyze our data, we employ six statistical indicators: the mean signed error (MSE), the mean absolute error (MAE), the root-mean-square error (RMSE), the standard deviation of errors (SDE), the mean signed percentage error (MSPE), and the mean absolute percentage error (MAPE), defined as follows

$$\text{MSE} = \frac{1}{N} \sum_{i=1}^N (y_i^{\text{cur.}} - y_i^{\text{ref.}}) \quad (2a)$$

$$\text{MAE} = \frac{1}{N} \sum_{i=1}^N |y_i^{\text{cur.}} - y_i^{\text{ref.}}| \quad (2b)$$

$$\text{RMSE} = \sqrt{\frac{1}{N} \sum_{i=1}^N (y_i^{\text{cur.}} - y_i^{\text{ref.}})^2} \quad (2c)$$

$$\text{SDE} = \sqrt{\frac{1}{N} \sum_{i=1}^N (y_i^{\text{cur.}} - \text{MSE})^2} \quad (2d)$$

$$\text{MSPE} = \frac{1}{N} \sum_{i=1}^N \frac{(y_i^{\text{cur.}} - y_i^{\text{ref.}})}{y_i^{\text{ref.}}} \quad (2e)$$

$$\text{MAPE} = \frac{1}{N} \sum_{i=1}^N \frac{|y_i^{\text{cur.}} - y_i^{\text{ref.}}|}{y_i^{\text{ref.}}} \quad (2f)$$

where $y_i^{\text{cur.}}$ and $y_i^{\text{ref.}}$ are the current and reference values of the i th transition/state, respectively, and N is the total number of transitions/states.

The majority of transitions considered here are of predominantly single excitation character ($\%T_1 > 85\%$), based on our reference CC3/dAVTZ calculations. The few states with $\%T_1 > 85\%$ are listed in Table 1. While CC3 is likely less accurate for these states, $\%T_1$ remains rather high in all cases. All states are fully characterized in the SI.

A challenge encountered when computing reference values is state characterization as, in some cases, the orbital composition of a given state may change significantly with the basis set extension. To assign unambiguously the computed ES, we

Table 1. States Included in This Study Exhibiting Relatively Low Single Excitation Character ($\%T_1 > 85\%$)^a

molecule	state	$\Delta E_{0,n}$	$\%T_1$
acrolein	2A'' (V, n-π*)	6.743	79.5
cyclopentadiene	2A ₁ (V, π-π*)	6.567	78.3
glyoxal	2B _g (V, n-π*)	6.566	84.0
tetrazine	1B _{1g} (V, n-π*)	4.910	83.1
	1B _{2g} (V, n-π*)	5.463	81.8

^aBoth energy (in eV) and $\%T_1$ were obtained from our reference CC3/dAVTZ calculations. All states have a valence (V) character.

initially calculated CC3/AVDZ values and compared them with the values of the QUEST database, followed by CC3/dAVTZ values, which were compared to the AVDZ results. In cases where assignment was not possible based solely on GSA f and vertical excitation energy ($\Delta E_{0,n}$), it was necessary to analyze the orbital composition. Occasionally, some states became too mixed when going from AVDZ to dAVTZ, or *vice versa*. This issue was particularly common for energetically higher-lying states. For example, the $1\Pi_u$ state of N₂ and the $3A_1$ state of formaldehyde exhibit significant state mixing upon removal/addition of diffuse functions. Transitions involving such mixed states were excluded from our set, as their character was too ambiguous for a reliable characterization.

To characterize the states determined on the optimal S₁ or S₂ geometries, we compared the orbital composition of the states obtained on the ground- and excited-state structures. For formaldehyde, the point group changes when going from the S₀ (C_{2v}) to the S₁ (C_s) geometry. Nonetheless, after visualizing the corresponding orbitals, we were able to match the (C_s) states to their (C_{2v}) counterparts. The correspondences are detailed in Table S49 of the SI.

Some molecules have a non-Abelian point group symmetry. The majority of quantum chemistry program packages, including the ones we employed, cannot perform calculations in a non-Abelian point group. In these cases, the program descends to a lower-symmetry point group, that is, the highest-symmetry Abelian point group. This can lead to arbitrary degeneracies when an irreducible representation of the original non-Abelian point group corresponds to two possible irreducible representations in the new lower-symmetry Abelian point group. The two degenerate states have the same f , μ , and $\Delta E_{0,n}$. To obtain the f (μ) values of the original state, one has to sum up the corresponding degenerate values of f (μ), i.e., multiply them by two. In the case of ESA, if both states involved in the transition are degenerate, one has to multiply the corresponding value of f (μ) by four. In this work, we publish f (μ) of only one of the degenerate states/transitions, and we highlight the degenerate states with an asterisk (*).

3.1. Reference Values. To select an appropriate reference basis set, we study the small set of transitions provided in Table 2 using the very large d-aug-cc-pVQZ basis. All states taking part in these transitions have a predominantly single excitation character (%T₁ > 85%). The MSE, MAE, RMSE,

and SDE of μ and f computed with different basis sets at the QR-CC3 level are given in Figure 2. The data clearly underscore the importance of double augmentation on both f and μ values, as well as the very similar error patterns for these two properties.

While the reduction in MAE achieved by expanding the AVDZ basis set with respect to ζ is only marginal (MAEs for f of 0.061, 0.055, and 0.047 for AVDZ, AVTZ, and AVQZ, respectively), further augmenting the basis with diffuse functions brings a significant improvement (MAEs for f of 0.061, 0.008, and 0.008 for AVDZ, dAVDZ, and tAVDZ, respectively). The significant effect of additional diffuse functions stems from the fact that most of the transitions in this comparison include at least one state of Rydberg character. Using a triply augmented basis set (tAVDZ or tAVTZ) changes the results only marginally and is, therefore, unnecessary. This further justifies the choice of a doubly augmented basis set as a reference as opposed to a triply augmented one.

Additionally, the differences between MAE and SDE, and MAE and RMSE, are much smaller in the case of doubly-(triply-)augmented basis sets hinting at a rather systematic error pattern.

As stated above, the trends in f and μ values are consistent. This should be the case since f is proportional to μ . However, unlike μ , f is influenced by the computed energy difference, which can introduce an additional source of error. Nevertheless, given the data in Figure 2, we focus solely on comparing f below.

To further confirm the quality of QR-CC3/dAVTZ values, we investigate gauge invariance at this level of theory. It can be clearly seen in Table 3 that the choice of gauge is insignificant as MAE, RMSE, and SDE are all lower than 0.005, and the MAPE is smaller than 0.1. Therefore, according to the gauge invariance metrics, the f values obtained at this level of theory are very accurate.

Looking at the convergence of different gauges for all QR-CC approaches (see Table S40 in SI), we found three outcomes: (i) the deviation of the velocity and mixed gauges from the length one is minimal at the QR-CC3 level; (ii) the deviation of the mixed gauge from the length one decreases when one increases the level of theory, that is, QR-CC2 > QR-CCSD > QR-CC3; (iii) the velocity gauge values obtained with QR-CCSD deviate from their length counterparts significantly more than in the case of QR-CC2. While investigating this last unexpected outcome, we found that, in a few cases, when the f determined with QR-CCSD in the velocity gauge differs significantly from the length one, the values of the velocity transition dipole moments of the left and right eigenvectors differ to a great extent. The reason behind this behavior remains unclear.

For additional verification, we extrapolated the oscillator strengths using a second-degree polynomial to obtain FCI estimates, as described in Sec. 2. We examined the $1A_2 \rightarrow 1B_1$ transition of water, the $2\Sigma^+ \rightarrow 3\Sigma^+$ and $1\Pi \rightarrow 2\Pi$ transitions of carbon monoxide, as well as the $1A_2 \rightarrow 1E$ and $1A_2 \rightarrow 2A_1$ transitions of ammonia. The extrapolated FCI results within the dAVDZ basis are summarized in Table 4, where they are compared with CC3 values. The CC3 results exhibit an excellent agreement with extrapolated FCI values, with a maximum deviation of 0.006 observed for the $1\Pi \rightarrow 2\Pi$ transition of the carbon monoxide using the length gauge.

Table 2. Selected Transitions with Corresponding Reference Values for $\Delta E_{m,n}$ (in eV) and f (in Length Gauge) Obtained at the CC3/dAVQZ^a

molecule	initial state	final state	$\Delta E_{m,n}$	f
ammonia	1A ₂ (R)	1E (R)*	1.547	0.319
	1A ₂ (R)	2A ₁ (R)	1.995	0.294
	1E (R)*	2A ₂ (R)	1.006	0.134
	2A ₁ (R)	2A ₂ (R)	0.558	0.264
CO	2Σ ⁺ (R)	3Σ ⁺ (R)	0.609	0.146
	2Σ ⁺ (R)	2Π (R)*	0.737	0.255
	2Π (R)*	1Π (V)*	2.986	0.010
diazirine	1B ₁ (V)	2A ₁ (V)	3.909	0.014
	1B ₂ (R)	2A ₁ (V)	0.537	0.080
silylidene	1A ₂ (V)	1B ₂ (V)	1.626	0.003
water	1B ₁ (R)	1A ₂ (R)	1.768	0.281

^aV = valence, R = Rydberg. The asterisks highlight degenerate states (see main text).

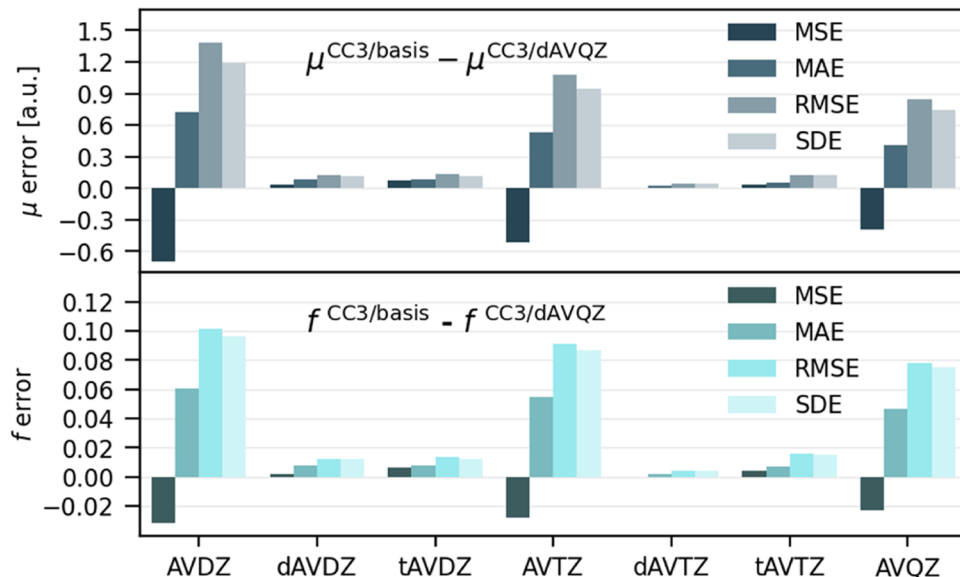


Figure 2. MSE, MAE, RMSE, and SDE of μ (top) and f in length gauge (bottom), computed with seven different basis sets (AVDZ, dAVDZ, tAVDZ, AVTZ, dAVTZ, tAVTZ, and AVQZ) and QR-CC3. QR-CC3/dAVQZ is used as a reference.

Table 3. MSE, MAE, RMSE, and SDE Associated with Oscillator Strengths (f) Obtained in the Velocity and Mixed Gauges (CC3/dAVTZ)^a

gauge	MSE	MAE	RMSE	SDE
velocity	0.0018	0.0021	0.0043	0.0039
mixed	0.0009	0.0011	0.0021	0.0019

^a f values obtained in the length gauge at the CC3/dAVTZ level serve as our reference.

Table 4. Extrapolated FCI (exFCI) and CC3 Oscillator Strengths of the $1A_2 \rightarrow 1B_1$ Transition of Water, the $2\Sigma^+ \rightarrow 3\Sigma^+$ and $1\Pi \rightarrow 2\Pi$ Transitions of Carbon Monoxide, and the $1A_2 \rightarrow 1E$ and $1A_2 \rightarrow 2A_1$ Transitions of Ammonia, Calculated in the dAVDZ Basis Set

molecule	transition	exFCI	CC3
water	$1A_2 \rightarrow 1B_1$	f^l	0.2897(4)
		f^v	0.2853(1)
		f^m	0.2875(3)
CO	$2\Sigma^+ \rightarrow 3\Sigma^+$	f^l	0.0109(0)
		f^v	0.0082(2)
		f^m	0.0095(2)
CO	$1\Pi \rightarrow 2\Pi$	f^l	0.1405(9)
		f^v	0.152(2)
		f^m	0.1466(5)
ammonia	$1A_2 \rightarrow 1E$	f^l	0.3229(0)
		f^v	0.3223(0)
		f^m	0.3226(0)
ammonia	$1A_2 \rightarrow 2A_1$	f^l	0.2972(0)
		f^v	0.2968(1)
		f^m	0.2970(0)

3.2. Basis Set Effects. After establishing that the dAVTZ basis set is sufficiently large for computing oscillator strengths, we explore the effects of using smaller basis sets. We examine the f values obtained with AVDZ, dAVDZ, and AVTZ at the QR-CC3, QR-CCSD, QR-CC2, and ISR-ADC(2) levels of theory, comparing them to the corresponding dAVTZ values. By excluding the computationally demanding triple-augmented

and quadruple- ζ basis sets, we were able to include in this comparison all 53 transitions, listed in Table 5. QR-CC3 and ISR-ADC(2) statistical values obtained with different basis sets are shown in Figure 3. Additional results can be found in the SI (Tables S41 and S42).

Upon looking at the QR-CC3 results, one can see that the trends are consistent with the findings obtained for the smaller set of transitions (see above). In particular, the augmentation with extra diffuse functions is more crucial than increasing ζ -multiplicity. Indeed, the AVTZ results (MAE = 0.017, RMSE = 0.042, and SDE = 0.040) do not significantly differ from their AVDZ counterparts (MSE = 0.020, RMSE = 0.047, and SDE = 0.045). On the other hand, the dAVDZ results (MAE = 0.004, RMSE = 0.007, and SDE = 0.007) are much closer to the reference values than their singly augmented AVDZ equivalents.

We further divide the QR-CC3 results based on the nature of states involved in the transition (Figure 4): Rydberg–Rydberg, Rydberg-valence, and valence–valence. For the first category of transitions, the trend remains consistent with the pattern observed when all transitions are considered together, which is expected as the majority of transitions, 34 out of 53, are of Rydberg–Rydberg nature. Examining the Rydberg-valence and valence–valence transitions reveals that the importance of additional diffuse functions diminishes, as anticipated, with a clear preference for higher ζ -multiplicity over extra diffuse functions in the case of ESA between two valence states. Additionally, the errors determined at QR-CC3 level decrease across the transition types, following the series Rydberg–Rydberg \rightarrow Rydberg-valence \rightarrow valence–valence. This error reduction is more pronounced with the singly augmented basis sets, whereas only a slight improvement is observed with dAVDZ. Overall, the MAE in f at the QR-CC3 level remains consistently small across different basis sets, not exceeding 0.03.

We also investigate basis set effects at lower levels of theory by comparing f values computed with AVDZ, dAVDZ, and AVTZ at the QR-CCSD, QR-CC2, and ISR-ADC(2) levels, against their corresponding dAVTZ values obtained at the

Table 5. Full List of CC3/dAVTZ Transitions between State n and State m ^a

molecule	initial state n			final state m			transition			
	state	$\Delta E_{0,n}$	%T ₁	state	$\Delta E_{0,m}$	%T ₁	$\Delta E_{m,n}$	f ^l	f ^v	f ^m
acetone	1B ₂ (R)	6.418	90.6	2A ₁ (R)	7.450	90.6	1.032	0.256	0.259	0.257
	1B ₂ (R)	6.418	90.6	2B ₂ (R)	7.456	91.1	1.037	0.267	0.268	0.268
	1B ₂ (R)	6.418	90.6	2A ₂ (R)	7.382	91.0	0.964	0.361	0.364	0.363
acrolein	1A'' (V)	3.741	87.6	2A'' (V)	6.743	79.5	3.002	0.036	0.039	0.037
ammonia	1A ₂ (R)	6.572	93.5	1E (R) *	8.117	93.7	1.545	0.320	0.321	0.321
	1A ₂ (R)	6.572	93.5	2A ₁ (R)	8.564	93.4	1.992	0.295	0.296	0.296
	1E (R) *	8.117	93.7	2A ₂ (R)	9.121	93.6	1.003	0.139	0.143	0.141
benzene	2A ₁ (R)	8.564	93.4	2A ₂ (R)	9.121	93.6	0.556	0.252	0.278	0.264
	1E _{1g} (R) *	6.504	92.8	1A _{2u} (R)	7.053	93.5	0.549	0.132	0.133	0.133
	1E _{1g} (R) *	6.504	92.8	1E _{2u} (R) *	7.117	92.9	0.613	0.138	0.140	0.139
butadiene	1B _g (R)	6.310	94.2	1A _u (R)	6.626	94.1	0.316	0.122	0.124	0.124
	1B _g (R)	6.310	94.2	2A _u (R)	6.780	94.1	0.470	0.165	0.167	0.166
	1A _u (R)	6.626	94.1	2B _g (R)	7.447	94.4	0.821	0.062	0.062	0.062
carbon monoxide	2A _u (R)	6.780	94.1	2B _g (R)	7.447	94.4	0.667	0.367	0.369	0.368
	2Σ ⁺ (R)	10.676	91.8	3Σ ⁺ (R)	11.285	92.4	0.609	0.146	0.146	0.147
	2Σ ⁺ (R)	10.676	91.8	2Π (R) *	11.414	92.4	0.738	0.256	0.261	0.258
cyclopentadiene	2Π (R) *	11.414	92.4	1Π (V) *	8.481	93.1	2.933	0.010	0.009	0.009
	2Σ ⁺ (R)	10.676	91.8	1Π (V) *	8.481	93.1	2.195	0.025	0.025	0.025
	3Σ ⁺ (R)	11.285	92.4	1Π (V) *	8.481	93.1	2.804	0.010	0.010	0.010
cyclopropene	1B ₂ (V)	5.538	93.8	2A ₁ (V)	6.567	78.3	1.029	0.023	0.032	0.027
	1A ₂ (R)	5.759	94.0	1B ₁ (R)	6.375	94.2	0.616	0.235	0.236	0.236
	1A ₂ (R)	5.759	94.0	2B ₂ (R)	6.448	94.3	0.689	0.282	0.284	0.283
diazomethane	1A ₂ (R)	5.759	94.0	2A ₂ (R)	6.412	93.9	0.653	0.252	0.254	0.253
	2B ₁ (R)	6.921	95.2	3B ₁ (R)	7.294	95.1	0.373	0.103	0.102	0.103
	1B ₁ (V)	4.113	92.5	2A ₁ (V)	7.972	93.8	3.859	0.014	0.015	0.014
formaldehyde	1B ₂ (R)	7.442	93.5	2A ₁ (V)	7.972	93.8	0.530	0.085	0.084	0.084
	1A ₂ (V)	3.071	90.1	1B ₁ (R)	5.436	93.8	2.364	0.012	0.012	0.012
	1B ₂ (R)	7.173	91.7	2A ₁ (R)	8.144	92.0	0.972	0.297	0.301	0.299
furane	1A ₂ (V)	3.968	91.5	2A ₂ (R)	8.386	92.0	1.214	0.278	0.279	0.279
	1A ₂ (R)	7.173	91.7	1B ₂ (R)	7.173	91.7	3.205	0.019	0.020	0.020
	1A ₂ (V)	3.968	91.5	2A ₂ (R)	8.386	92.0	0.392	0.011	0.011	0.011
glyoxal	1A ₂ (V)	3.968	91.5	2A ₂ (R)	8.386	92.0	4.419	0.015	0.014	0.014
	1A ₂ (R)	6.061	93.8	2B ₂ (R)	6.883	93.8	0.822	0.271	0.272	0.271
	1A ₂ (R)	6.061	93.8	1B ₁ (R)	6.606	93.9	0.544	0.220	0.220	0.220
ketene	1A ₂ (R)	6.061	93.8	2A ₂ (R)	6.754	93.8	0.693	0.268	0.269	0.269
	1B ₁ (R)	5.948	93.9	1B _g (V)	4.267	88.3	1.393	0.020	0.021	0.021
	1A ₂ (V)	2.874	91.0	2B _g (V)	6.566	84.0	3.692	0.113	0.117	0.115
Mcp	1B ₁ (R)	5.948	93.9	2A ₂ (R)	7.109	94.3	1.161	0.336	0.338	0.337
	1B ₂ (V)	4.311	85.5	2A ₁ (V)	7.085	92.9	1.136	0.176	0.174	0.175
	1B ₁ (R)	5.422	93.6	1A ₂ (R)	5.928	93.3	0.506	0.188	0.189	0.189
pyrazine	2A _g (R)	6.638	91.1	1A ₂ (R)	5.928	93.3	1.616	0.023	0.025	0.024
	2A _g (R)	6.638	91.1	2B _{1u} (R)	7.409	91.5	0.771	0.198	0.197	0.198
	1B _{1u} (V)	7.409	91.5	2B _{2u} (R)	7.229	90.8	0.591	0.240	0.244	0.242
pyridazine	2B _{2u} (R)	7.229	90.8	1B _{3g} (R)	7.951	91.2	1.090	0.004	0.004	0.004
	1A ₂ (V)	4.372	86.9	2B ₁ (V)	6.366	87.0	1.995	0.012	0.010	0.011
	1A ₂ (R)	5.233	92.9	1B ₁ (R)	5.967	92.6	0.734	0.091	0.091	0.091
pyrrole	1A ₂ (R)	5.233	92.9	2A ₂ (R)	5.980	93.0	0.747	0.171	0.171	0.171
	1A ₂ (V)	2.155	88.0	1B ₂ (V)	3.780	92.3	1.624	0.003	0.002	0.003
	1B _{3u} (V)	2.454	89.8	1B _{1g} (V)	4.910	83.1	2.456	0.061	0.068	0.065
silylidene	1B _{3u} (V)	2.454	89.8	1B _{2g} (V)	5.463	81.8	3.009	0.017	0.017	0.017
	1A ₂ (R)	6.121	92.7	1B ₁ (R)	6.131	90.1	0.009	0.001	-0.004	0.000
	water	7.600	93.4	1A ₂ (R)	9.368	93.5	1.768	0.283	0.284	0.283

^aTransitions energies $\Delta E_{0,m}$, $\Delta E_{0,mm}$ and $\Delta E_{m,n}$ (in eV), the percentage of single excitation character (%T₁) of the two states and ESA oscillator strengths in length, velocity and mixed gauges, f^l, f^v and f^m, respectively. Rydberg = R, valence = V. The asterisks highlight degenerate states (see main text).

same level of theory. We show here only the ISR-ADC(2) example in Figure 3. In all cases, we found that including

additional diffuse functions is more crucial than increasing ζ -multiplicity, which is consistent with our findings at the QR-

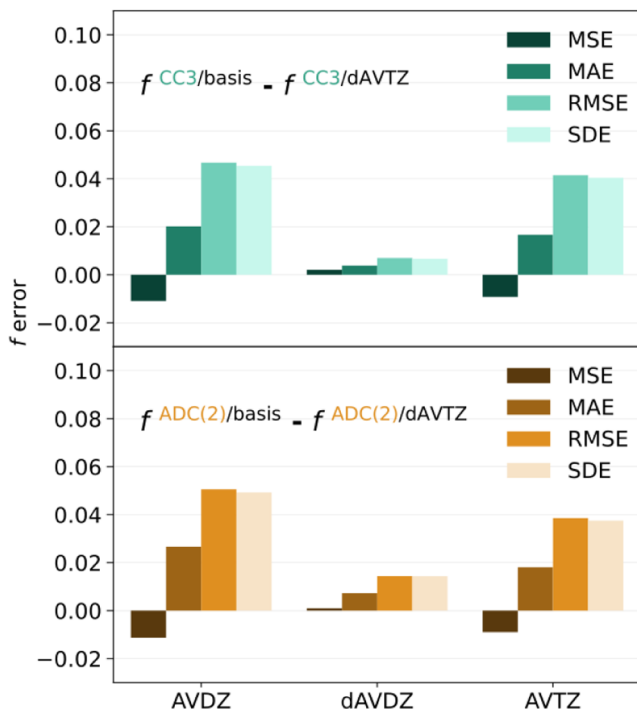


Figure 3. MSE, MAE, RMSE, and SDE of f_f in length gauge, computed with three different basis sets (AVDZ, dAVDZ, and AVTZ). Top: CC3 results compared with CC3/dAVTZ; bottom: ADC(2) results compared with ADC(2)/dAVTZ.

CC3 level of theory (see above). The trend remains consistent when comparing the ISR-ADC(2) values obtained with different basis sets to our reference CC3/dAVTZ data. The MAEs diminish across ISR-ADC(2)/AVDZ (MAE = 0.037), ISR-ADC(2)/AVTZ (MAE = 0.030), ISR-ADC(2)/dAVDZ (MAE = 0.026), ISR-ADC(2)/dAVTZ (MAE = 0.022), as expected.

At this stage, we would like to mention that the QR-CC3/dAVTZ calculations are extremely computationally demanding. This issue could be alleviated by employing the dAVDZ basis set instead of dAVTZ, as the errors at the QR-CC3 level remain relatively small. Indeed, in our full testing set of 53 transitions, the largest deviation of f_f between results obtained with dAVDZ and dAVTZ occurs for the $1A_2$ (Rydberg, π -3s) $\rightarrow 1B_1$ (Rydberg, π -3p) transition of thiophene where the QR-CC3/dAVTZ (dAVDZ) f_f is 0.001 (0.023). Clearly, it is not a chemically significant deviation as both values of f_f would characterize the transition as a low-intensity one. Nevertheless, we note that this deviation is not due to state mixing caused by basis set expansion as an examination of the orbital compositions for both states with both basis sets revealed no substantial state mixing. We opted to stick with the larger dAVTZ basis for the remainder of this study.

3.3. Methods Benchmark. We compare the errors in (length gauge), $\Delta E_{0,n}$, and $\Delta E_{m,n}$ obtained with all methods (dAVTZ basis set) against QR-CC3/dAVTZ in Figure 5. The $\Delta E_{0,n}$ values correspond to the GSA vertical transition energies (71 excited states) and $\Delta E_{m,n} = \Delta E_{0,n} - \Delta E_{0,m}$ corresponds to the difference of the two GSA values involved in the corresponding ESA transition (53 transitions). The MAEs of f_f for the wave function methods grow in the series: QR-CCSD (0.006), ISR-ADC(3) (0.009), EOM-CCSD (0.009), QR-CC2 (0.020), and ISR-ADC(2) (0.022). We see that QR-CCSD is

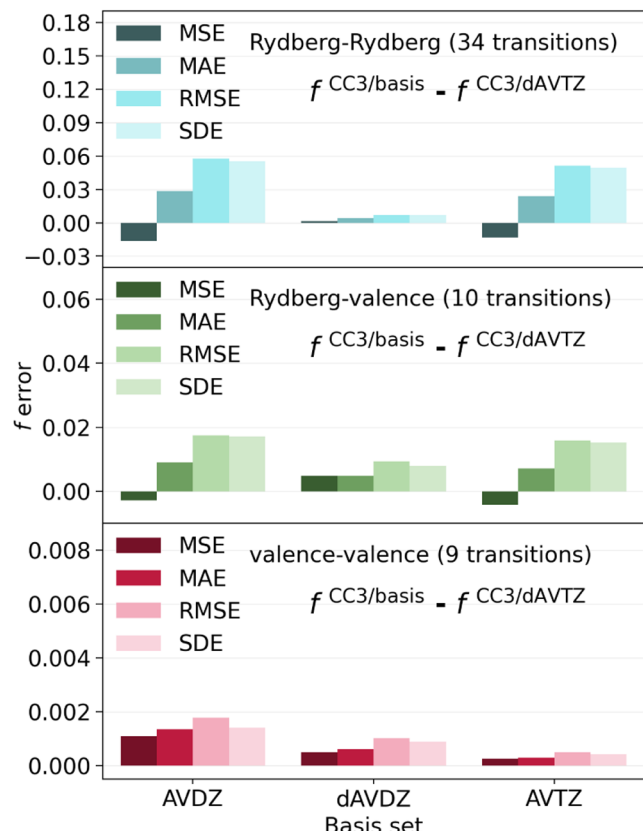


Figure 4. MSE, MAE, RMSE, and SDE of f_f in length gauge, computed with different basis sets at the CC3 level of theory for various sets of transitions: Rydberg–Rydberg (top), Rydberg–valence (center), and valence–valence (bottom). The reference values are obtained at the CC3/dAVTZ level. Note the difference in the scales of the vertical axis.

the closest to our reference, with EOM-CCSD and ISR-ADC(3) only slightly behind. We would like to stress the excellent performance of ISR-ADC(3) which yields results comparable to EOM-CCSD, consistent with previous findings for GSA by some of us.³⁴ While ADC(3) is not always trustworthy for transition energies from the ground state (see below), it can provide accurate properties. When we compare the MAE in $\Delta E_{m,n}$ with the MAE in $\Delta E_{0,n}$, we see that the errors are smaller for $\Delta E_{m,n}$ than for $\Delta E_{0,n}$, which is logical since the GSA energy differences are often larger than the ESA ones. This is beneficial for calculating ESA f_f values, as they are computed from μ and $\Delta E_{m,n}$ rather than $\Delta E_{0,n}$, as in the case of GSA f_f values. The difference between the MAEs of $\Delta E_{0,n}$ and $\Delta E_{m,n}$ for the wave function approaches grows across the following series: CCSD (0.069 eV), CC2 (0.083 eV), ADC(2) (0.085 eV), and ADC(3) (0.114 eV). At this stage, it is worth reminding that the energies obtained with QR-CCSD and EOM-CCSD are identical within numerical error. The RMSE and SDE in f_f obtained from the wave function approaches are very close to the MAE values, with ISR-ADC(3) and second-order approaches [QR-CC2 and ISR-ADC(2)] giving larger deviations between these statistical indicators. This is an important feature of these methods indicating rather systematic errors, tight error distributions, and low frequency of outliers. This is in contrast with QR-TDDFT, as discussed below.

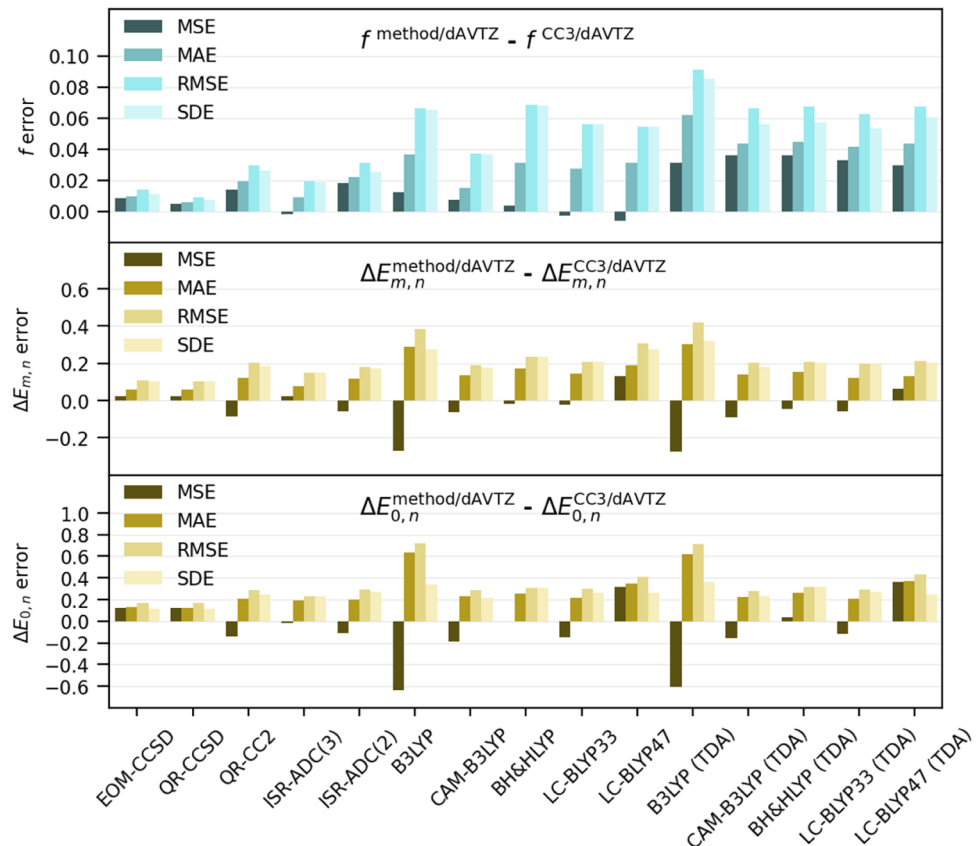


Figure 5. Comparison of MSE, MAE, RMSE, and SDE for all methods. Top: f in length gauge; center: $\Delta E_{m,n}$ in eV; bottom: $\Delta E_{0,n}$ in eV. $\Delta E_{m,n}$ and f values are compared with QR-CC3/dAVTZ and $\Delta E_{0,n}$ with CC3/dAVTZ.

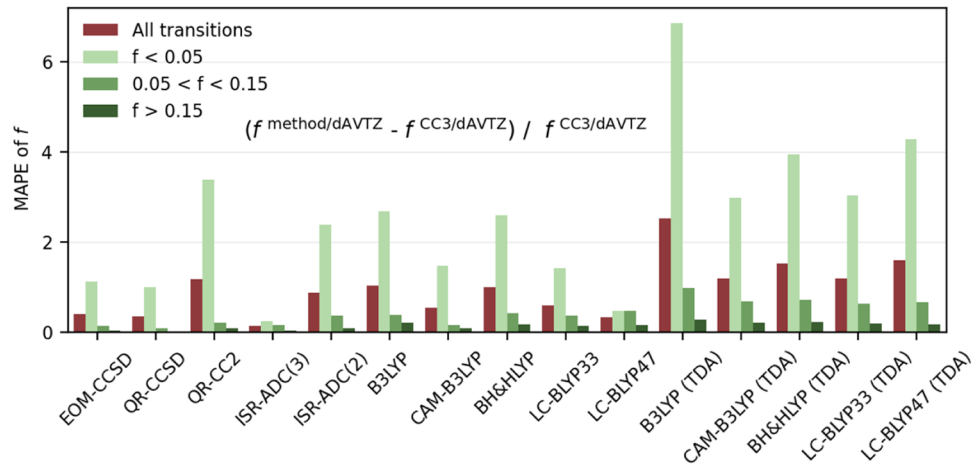


Figure 6. Comparison of MAPE in f values of all methods divided by the magnitude of the computed f into three groups: $f < 0.05$, $0.05 < f < 0.15$, and $f > 0.15$. The reference values are obtained at the CC3/dAVTZ level in length gauge.

Upon analyzing the QR-TDDFT results, two general features become apparent. First, the difference between the RMSE and MAE values of f is larger than those observed with wave function approaches. The same holds for the differences between SDE and MAE. As mentioned earlier, this behavior is in stark contrast with wave function approaches and has been reported by some of us previously for two-photon absorption cross sections computed with QR-TDDFT.⁷⁶ This highlights a key characteristic of QR-TDDFT: it can produce highly accurate transition properties, yet it may also yield significantly inaccurate results. The second feature is the impact of the

TDA on the calculated f values and transition energies. While the TDA offers a reduction in computational cost, this comes at the expense of a noticeable deterioration in the computed f values, as reflected by an increase in the MAE. The magnitude of this effect depends on the XCF. Nevertheless, the ranking of functionals, based on the MAE of f , remains relatively consistent between full TDDFT and TDA calculations. For full TDDFT, the ranking is as follows: CAM-B3LYP (0.015), LC-BLYP33 (0.027), LC-BLYP47 (0.031), BH&HLYP (0.031), and B3LYP (0.036). For TDA, the ranking becomes

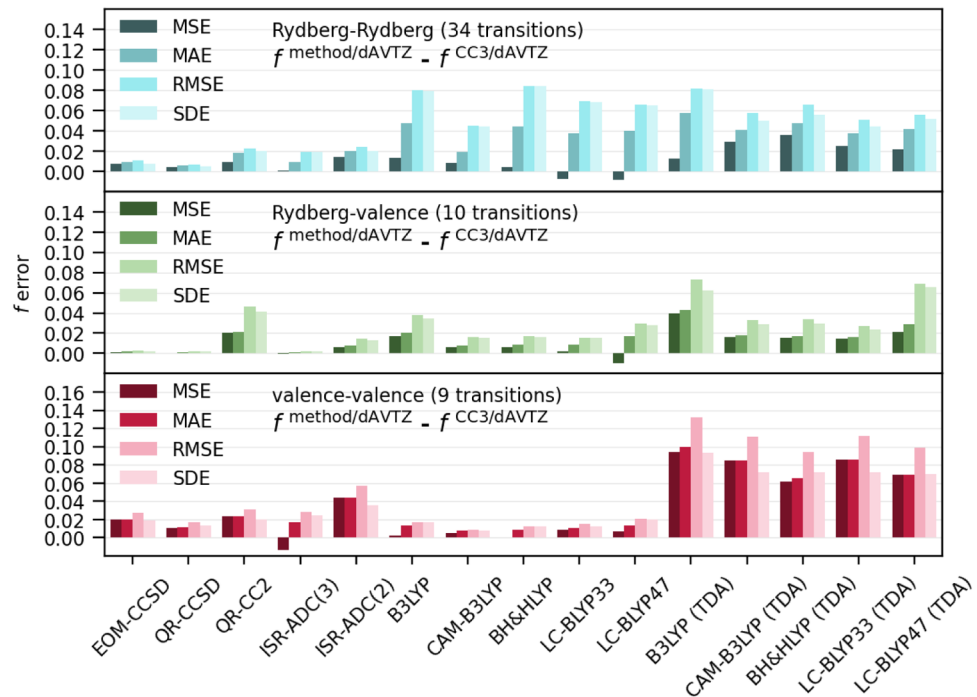


Figure 7. Comparison of errors in f for all methods divided by the character of the states involved. Top: Rydberg–Rydberg; center: Rydberg–valence; bottom: valence–valence. See the caption of Figure 5 for more details.

LC-BLYP33 (0.042), CAM-B3LYP (0.044), LC-BLYP47 (0.044), BH&HLYP (0.045), and B3LYP (0.062).

Interestingly, the effect of the TDA originates, in practice, solely from the μ values as the differences between the energies obtained with and without TDA are negligible for ESA. Similarly to what we found for wave function approaches, the cancellation of errors introduced by the subtraction of $\Delta E_{0,n}$ indeed improves the $\Delta E_{m,n}$ values. The difference between the MAEs of $\Delta E_{0,n}$ and the MAEs of $\Delta E_{m,n}$ of the TDDFT approaches grows in the following series (see Table S45 in the SI): LC-BLYP33 (0.074 eV), TDA-CAM-B3LYP (0.080 eV), BH&HLYP (0.082 eV), TDA-LC-BLYP33 (0.084 eV), CAM-B3LYP (0.092 eV), TDA-BH&HLYP (0.106 eV), LC-BLYP47 (0.157 eV), TDA-LC-BLYP47 (0.243 eV), TDA-B3LYP (0.313 eV), and B3LYP (0.351 eV). While B3LYP largely undershoots the GSA energies in the present set, the errors become reasonable for the ESA energies.

From the analysis of all transitions, it is clear that CAM-B3LYP, without TDA, appears as the XCF of choice for computing ESA f values at the TDDFT level, with the lowest MAE (0.015), RMSE (0.037) and SDE (0.036) from all the tested functionals. The second best for ESA (f) is likely LC-BLYP33 with a MAE of 0.027, a RMSE of 0.056, and a SDE of 0.056. LC-BLYP47 provides rather similar errors (see the SI Table S44). Quite interestingly, CAM-B3LYP even outperforms both QR-CC2 and ISR-ADC(2) in terms of MAE but not for the SDE.

In short, it appears that QR-TDDFT may deliver average errors similar to, or even smaller than, those of second-order wave function methods when an adequate functional is selected. However, the spread of the errors and the number of outliers remain larger with QR-TDDFT.

When one considers the MAPEs of f values instead of MAEs (see Figure 6), one finds that ISR-ADC(3) and LC-BLYP47 (without TDA) perform unexpectedly well. Specifically, ISR-

ADC(3) (MAPE = 0.132) outperforms all other methods while LC-BLYP47 (MAPE = 0.328) ranks highest among the tested XCFs. For the other methods, no significant deviations from the trends observed with MAEs were found. To further examine this outcome, we divided all transitions into three groups based on the magnitude of the computed f values: transitions with $f < 0.05$, transitions with $0.05 < f < 0.15$, and transitions with $f > 0.15$ (see Figure 6). While most methods show decreasing percentage errors as f increases, most notably for $f < 0.05$, this trend does not hold for ISR-ADC(3) and LC-BLYP47. For these two models, the MAPE remains nearly constant when transitioning from moderately bright transitions ($0.05 < f < 0.15$) to dark transitions ($f < 0.05$). This shows that ISR-ADC(3) and LC-BLYP47 perform both very well for transitions with (very) small f values, compared with the other tested methods. The reason behind this unexpected outcome remains unclear to us. Since real-life applications are mostly interested in bright ESA transitions with large f values, it is likely of limited practical interest.

To further characterize the performance of all methods, we divided the transitions by the character of states involved: Rydberg–Rydberg, Rydberg–valence, and valence–valence; as well as by the molecular size: molecules containing 1 to 3 non-hydrogen atoms, and molecules containing 4 to 6 non-hydrogen atoms (see Figure 1).

When looking at the influence of the nature of the states on f values (Figure 7), one observes that the performance of QR-TDDFT (without TDA) improves as valence states are included in the ESA transition. The RMSE and SDE become comparable with the MAE. This is expected, as first, the valence states are generally easier to model, and second, the amount of transitions involving valence states is lower, 10 Rydberg–valence and 9 valence–valence compared with 34 Rydberg–Rydberg excitations, making it less likely for strong outliers to occur. Unexpectedly, we do not observe the same

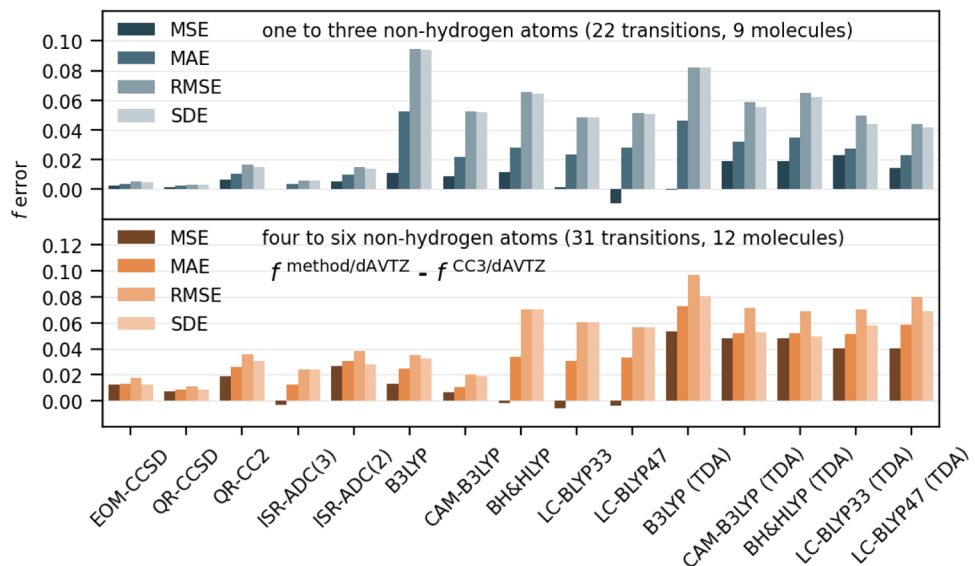


Figure 8. Comparison of errors in f for all methods depending on the molecular size. Top: 1–3 non-hydrogen atoms (22 transitions, 9 molecules); bottom: 4–6 non-hydrogen atoms (31 transitions, 12 molecules). See the caption of Figure 5 for more details.

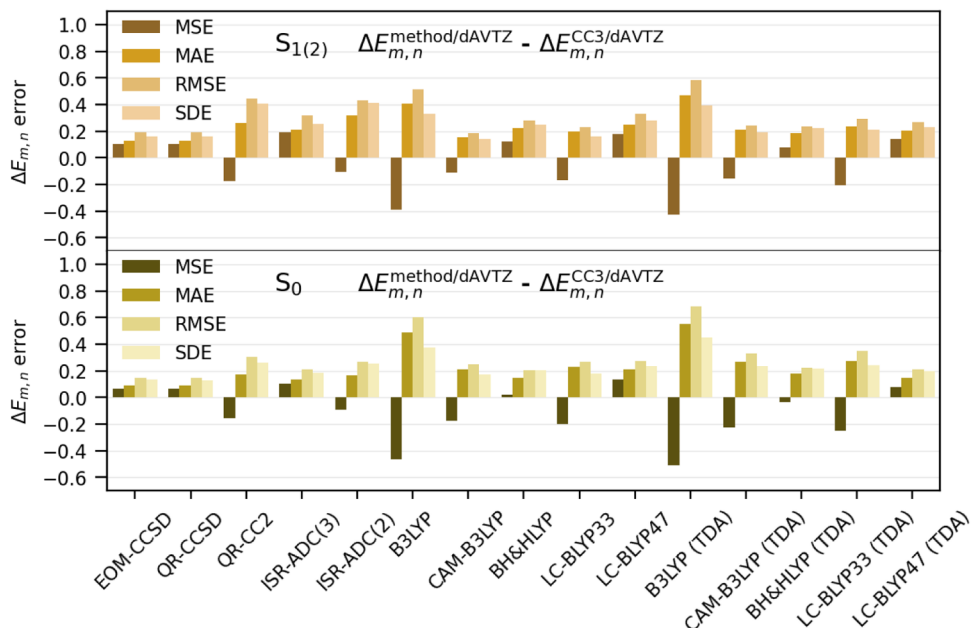


Figure 9. Comparison of MSE, MAE, RMSE, and SDE for $\Delta E_{m,n}$ in eV for all methods and a subset of transitions. Top: errors obtained on $S_{1/2}$ geometries; bottom: errors obtained on S_0 structures with the same subset of transitions. All values are compared with a CC3/dAVTZ reference. See the SI for raw data.

trend when the TDA is enforced, as the performance is slightly worse for valence–valence transitions than for the Rydberg–Rydberg ones, the lowest deviation being observed for the Rydberg–valence transitions. The wave function methods show the same trends. In fact, full TDDFT outperforms most of the wave function methods and is comparable to QR-CCSD when only valence–valence transitions are considered. Interestingly, BH&HLYP and B3LYP perform similarly for Rydberg–Rydberg transitions although one would expect BH&HLYP, a global hybrid with 50% of exact exchange, to perform much better for Rydberg states than B3LYP, a global hybrid with 20% of exact exchange. Indeed, it is well-known that global hybrids with a low percentage of exact exchange tend to perform poorly at larger interelectronic distances due to the

wrong behavior of the exchange-correlation kernel.^{77,78} In practice, the interesting, bright ESA transitions often involve states with significant Rydberg character. Indeed, in our set, only one valence–valence transition exhibits f higher than 0.09 (the $1B_g \rightarrow 1A_u$ transition of glyoxal).

Upon investigating the effect of system size on the computed f values (Figure 8), three important trends emerge. First, wave function methods perform in general worse for larger molecules, especially second-order methods, as upon increasing the system size the MAE of QR-CC2 [ISR-ADC(2)] grows from 0.010 (0.010) to 0.026 (0.031). Second, the impact of the TDA becomes more significant for larger systems: the TDA errors increase for larger molecules. Third, with the exception of both B3LYP and CAM-B3LYP, the MAE, RMSE, and SDE

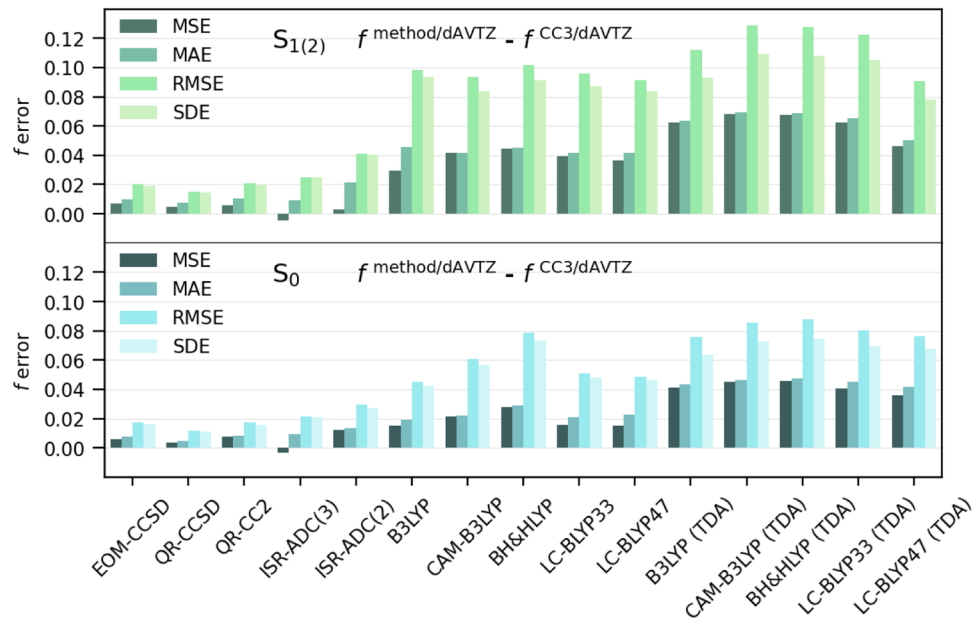


Figure 10. Comparison of MSE, MAE, RMSE, and SDE for f in length gauge for all methods and a subset of transitions. Top: errors obtained on $S_{1/2}$ geometries; bottom: errors obtained on S_0 structures with the same subset of transitions. All values are compared with a QR-CC3/dAVTZ reference. For full results see SI.

of all XCFs generally increase, or do not change significantly, for larger molecules. Upon increasing the system size, the MAE of B3LYP (CAM-B3LYP) decreases from 0.053 (0.022) to 0.025 (0.010). When we compare the change in SDE and RMSE, we see a similarly strong effect as for the MAE. In the case of CAM-B3LYP, for small molecules, one has SDE = 0.052 and RMSE = 0.053, which both decrease in larger compounds with SDE = 0.019 and RMSE = 0.020. For B3LYP, the improvements are even more significant: for smaller systems one has SDE = 0.094 and RMSE = 0.094 and, for larger compounds, SDE = 0.033 and RMSE = 0.035. The functional ranking, without TDA, thus changes dramatically for larger systems as B3LYP climbs up the performance ladder from the last place to the second one. Given that, as we mentioned before, in practical applications, the dyes used for ESA applications are rather large organic molecules, B3LYP does not seem to perform so badly after all. Most importantly, CAM-B3LYP, for larger systems, comes very close to wave function approaches and even outperforms ISR-ADC(3) (MAE = 0.013, RMSE = 0.024, and SDE = 0.024), ISR-ADC(2) (MAE = 0.031, RMSE = 0.039, and SDE = 0.028), CC2 (MAE = 0.026, RMSE = 0.036, and SDE = 0.031), and, in terms of MAE, EOM-CCSD (MAE = 0.013, RMSE = 0.018, and SDE = 0.013).

3.4. The Effect of Geometric Relaxation. Up to now we considered S_0 geometries only since our main focus is the computation of ESA oscillator strength in the Franck–Condon region. Nevertheless, it is relevant to discuss the effect of geometry relaxation on the computed properties since actual ESA often occurs on the ES potential energy surfaces. We selected a reasonable subset of 14 transitions determined on optimal S_1 or S_2 structures, for which we computed the ESA f (length gauge) and $\Delta E_{m,n}$ values with all methods with the dAVTZ atomic basis set. In more details, 13 transitions were computed on optimal S_1 geometries and 1 on an optimal S_2 geometry. To evaluate the errors of lower-order methods, we logically used the CC3/dAVTZ (S_1 or S_2) results as

benchmarks (see Tables S49 and S57 in the SI). We then compared the trends obtained for the same subset of transitions on the corresponding S_0 geometries. Indeed, given the compact nature of this subset, one cannot expect the statistical indicators nor the trends to perfectly match the one obtained above for the full set of 53 transitions. Therefore, our goal is to assess the differences between the ESA results obtained for the S_0 and $S_{1/2}$ geometries rather than selecting, e.g., an optimal XCF outside the Franck–Condon region.

Upon looking at the effect of geometry relaxation on the $\Delta E_{m,n}$ values (Figure 9) one notices that the errors of wave function approaches are slightly larger when using $S_{1/2}$ geometry than the S_0 one. The difference between the $S_{1/2}$ and S_0 energy MAE grows in the following series: CCSD (0.041 eV), ISR-ADC(3) (0.073 eV), QR-CC2 (0.088 eV), ISR-ADC(2) (0.151 eV). The overall trend in $\Delta E_{m,n}$ remains the same as at the Franck–Condon point. For full TDDFT, not only the magnitude of the errors is sensitive to the geometry, as expected,⁷⁹ but one also notes a strong dependence on the XCF. Indeed, while for BH&HYP and LC-BLYP47 (full TDDFT) the MAE slightly grows by 0.080 and 0.040 eV, respectively, as one moves from S_0 to $S_{1/2}$ structures, the reverse effect is found for B3LYP, CAM-B3LYP, and LC-BLYP33 with MAEs decreasing by -0.081, -0.055, and -0.028. The effect of TDA on the $\Delta E_{m,n}$ values remains rather subtle.

Let us now look at the ESA f values in length gauge (Figure 10). Going from S_0 to $S_{1/2}$ structures induces only a negligible deterioration of the performance of wave function methods, with the exception of ISR-ADC(2), but a significant drop in performance for TD(A)-TDDFT. The difference between the $S_{1/2}$ and S_0 f MAE of wave function methods grows in the following series: ISR-ADC(3) (0.000), QR-CCSD (0.002), EOM-CCSD (0.003), QR-CC2 (0.003), ISR-ADC(2) (0.008). The general trends are therefore unaffected by the selected geometry. For full TDDFT the increase of MAE (RMSE) at the $S_{1/2}$ geometry is BH&HYP: 0.016 (0.022), CAM-B3LYP:

0.020 (0.033), LC-BLYP47:0.020 (0.042), LC-BLYP33:0.021 (0.045), B3LYP: 0.026 (0.053), whereas for TDA, one gets: LC-BLYP47:0.009 (0.014), LC-BLYP33:0.020 (0.042), B3LYP: 0.021 (0.036), BH&HLYP: 0.022 (0.040), CAM-B3LYP: 0.023 (0.043). Given this nonuniform behavior of the XCFs the ranking of functionals based on MAE (full TDDFT), on this subset of transitions, changes from B3LYP (MAE = 0.020), LC-BLYP33 (MAE = 0.021), CAM-B3LYP (MAE = 0.022) and LC-BLYP47 (MAE = 0.022), BH&HLYP (MAE = 0.029) on S_0 geometry, to CAM-B3LYP (MAE = 0.042), LC-BLYP33 (MAE = 0.042), LC-BLYP47 (MAE = 0.042), BH&HLYP (MAE = 0.045), B3LYP (MAE = 0.046) on $S_{1/2}$ geometry. Therefore, from this limited subset, it appears that both LC-BLYP33 and CAM-B3LYP do provide valuable results on both structures, whereas the relative efficiency of B3LYP is strongly geometry-dependent. In short, all XCFs seem to yield larger errors when going away from the Franck–Condon region, and the trends in their performance can be significantly altered.

4. CONCLUSIONS

We have defined highly accurate reference values of $\Delta E_{m,n}$ and f values for a set of 53 excited-to-excited state (71 states) transitions in 21 small- and medium-sized molecules using the QR-CC3/dAVTZ level of theory and S_0 geometries. We confirmed the validity of this benchmark level by studying a small set of transitions in 5 compact molecules by comparison with (i) QR-CC3/dAVQZ, QR-CC3/AVQZ, QR-CC3/tAVTZ, and QR-CC3/tAVDZ values, (ii) differences between f obtained in different gauges, and (iii) extrapolated FCI results.

After verifying the quality of the QR-CC3/dAVTZ data, we explored the basis set effects for all transitions with three smaller basis sets: AVDZ, dAVDZ, and AVTZ. We found that, at the QR-CC3 level, augmentation with two sets of diffuse functions has a larger impact than ζ -multiplicity. This is because the majority of states considered in our study present a Rydberg character. The basis set dependences at the QR-CCSD, QR-CC2, and ISR-ADC(2) levels of theory are consistent with QR-CC3. We further found that, for the majority of the transitions, the dAVDZ basis is sufficient when QR-CC3 is used. This smaller basis set can thus be employed to establish reference values when the QR-CC3/dAVTZ approach becomes computationally out of reach.

Next we compared f , $\Delta E_{0,n}$, and $\Delta E_{m,n}$ obtained with six different wave function approaches: QR-CC3 (reference), QR-CCSD, EOM-CCSD, QR-CC2, ISR-ADC(2), and ISR-ADC(3) as well as QR-TDDFT with five different XCFs (B3LYP, CAM-B3LYP, BH&HLYP, LC-BLYP33, and LC-BLYP47) applying or not the TDA. We found that the MAE for f values obtained using wave function approaches follows the trend: QR-CCSD < ISR-ADC(3) < EOM-CCSD < QR-CC2 < ISR-ADC(2). Among the tested XCFs, CAM-B3LYP exhibited the best performance for ESA f in terms of MAE, followed by LC-BLYP33, LC-BLYP47, BH&HLYP, and B3LYP. The application of TDA is globally detrimental to the calculation of ESA oscillator strengths. Interestingly, ISR-ADC(3) and LC-BLYP47 (full TDDFT) give very accurate f values for low-intensity transitions.

We further found that TDDFT, without TDA, performs very well for valence–valence transitions and even outperforms some wave function approaches. However, since most bright ESA transitions studied here, include at least one Rydberg

state, this does not impact the overall statistics. The implication of this outcome for practical applications on large dyes remains an open question.

After investigating the effect of increasing the molecular size on the computed f values, we found that TDA introduces larger errors for larger molecules. Lastly, we discovered that the errors of (CAM-)B3LYP without TDA, become significantly smaller (and also more systematic) for the largest molecules of our set. For the other methods, the trend was the opposite. The (CAM-)B3LYP trends are advantageous as real-life dyes are, in general, large organic molecules, as we mentioned before.

In addition, a benchmark was performed for a subset of transitions using optimal ES geometries, and comparisons were made for the equivalent subset of transitions determined on the S_0 structures. We saw that the changes in $\Delta E_{m,n}$ errors are rather small upon leaving the Franck–Condon region. The same holds true for the ESA f results determined by wave function methods. However, for TD(A)-DFT, the impact of geometry change is large and the relative performances of XCFs is altered. Given the compact nature of the subset investigated, it is challenging to draw definitive conclusions on the best XCF for ESA calculations on ES structures. One can likely advise caution when computing ESA f outside the Franck–Condon region with TDDFT.

We saw that the behavior of QR-TDDFT is heavily dependent on the system (character of state, system size, GS or ES geometry). However, when computing ESA f on an optimal S_0 geometry, CAM-B3LYP seems to perform the best in the majority of cases, and we would therefore suggest relying on this XCF.

We would like to stress that all calculations were performed in the gas phase. In fact, to the very best of our knowledge, a robust solvation model for QR methods has yet to be implemented in any widely available computational chemistry software. Therefore, the development and implementation of a suitable solvation model would be a valuable addition, particularly for applications to real-life systems.

■ ASSOCIATED CONTENT

Supporting Information

The Supporting Information is available free of charge at <https://pubs.acs.org/doi/10.1021/acs.jctc.5c00159>.

Geometries for all compounds. Additional results for all methods and basis sets ([PDF](#))

■ AUTHOR INFORMATION

Corresponding Authors

Boris Le Guennic – CNRS, ISCR UMR 6226, Univ Rennes, F-35042 Rennes, France;  orcid.org/0000-0003-3013-0546; Email: Boris.Leguennic@univ-rennes.fr

Pierre-François Loos – CNRS, UPS, Laboratoire de Chimie et Physique Quantiques UMR 5626, Université de Toulouse, F-31062 Toulouse, France;  orcid.org/0000-0003-0598-7425; Email: loos@irsamc.ups-tlse.fr

Denis Jacquemin – CNRS, CEISAM UMR 6230, Nantes Université, F-44000 Nantes, France; Institut Universitaire de France (IUF), F-75005 Paris, France;  orcid.org/0000-0002-4217-0708; Email: Denis.Jacquemin@univ-nantes.fr

Authors

Jakub Širůček – CNRS, CEISAM UMR 6230, Nantes Université, F-44000 Nantes, France; CNRS, ISCR UMR 6226, Univ Rennes, F-35042 Rennes, France; orcid.org/0009-0004-9419-0411

Yann Damour – CNRS, UPS, Laboratoire de Chimie et Physique Quantiques UMR 5626, Université de Toulouse, F-31062 Toulouse, France

Complete contact information is available at:
<https://pubs.acs.org/10.1021/acs.jctc.5c00159>

Notes

The authors declare no competing financial interest.

ACKNOWLEDGMENTS

This work received financial support under the EUR LUMOMAT project and the Investment for the Future program ANR-18-EURE-0012, which supports the PhD thesis of JS. This research used resources from the GLICID Computing Facility (Ligerien Group for Intensive Distributed Computing 10.60487//glicid, Pays de la Loire, France). PFL and YD thank the European Research Council (ERC) under the European Union's Horizon 2020 research and innovation programme (Grant agreement No. 863481) for funding.

REFERENCES

- (1) Jailaubekov, A. E.; Willard, A. P.; Tritsch, J. R.; Chan, W.-L.; Sai, N.; Gearba, R.; Kaake, L. G.; Williams, K. J.; Leung, K.; Rossky, P. J.; Zhu, X.-Y. Hot Charge-Transfer Excitons set the Time Limit For Charge Separation at Donor/Acceptor Interfaces in Organic Photovoltaics. *Nat. Mater.* **2013**, *12*, 66–73.
- (2) Günes, S.; Neugebauer, H.; Sariciftci, N. S. Conjugated Polymer-Based Organic Solar Cells. *Chem. Rev.* **2007**, *107*, 1324–1338.
- (3) Samuel, I. D. W.; Turnbull, G. A. Organic Semiconductor Lasers. *Chem. Rev.* **2007**, *107*, 1272–1295.
- (4) Tang, C. W.; VanSlyke, S. A. Organic Electroluminescent Diodes. *Appl. Phys. Lett.* **1987**, *51*, 913–915.
- (5) Thomas, S. W.; Joly, G. D.; Swager, T. M. Chemical Sensors Based on Amplifying Fluorescent Conjugated Polymers. *Chem. Rev.* **2007**, *107*, 1339–1386.
- (6) Amarasinghe, D.; Ruseckas, A.; Vasdekis, A. E.; Turnbull, G. A.; Samuel, I. D. W. High-Gain Broadband Solid-State Optical Amplifier Using a Semiconducting Copolymer. *Adv. Mater.* **2009**, *21*, 107–110.
- (7) Baboola, C.; Narendran, N. S.; Pannipara, M.; Al-Sehemi, A. G.; Sabari Girisun, T. Excited State Absorption Assisted Optical Limiting Action of Fe Decorated γ -BBO Nanorods. *Mater. Chem. Phys.* **2019**, *237*, No. 121827.
- (8) Bellier, Q.; Makarov, N. S.; Bouit, P.-A.; Rigaut, S.; Kamada, K.; Feneyrou, P.; Berginc, G.; Maury, O.; Perry, J. W.; Andraud, C. Excited State Absorption: A Key Phenomenon for the Improvement of Biphotonic Based Optical Limiting at Telecommunication Wavelengths. *Phys. Chem. Chem. Phys.* **2012**, *14*, 15299–15307.
- (9) Han, Y.; Xiao, J.; Wu, X.; Wang, Y.; Zhang, X.; Song, Y. Synthesis and Ultrafast Broadband Optical Limiting Properties of a Two-Branched Twistacene. *Molecules* **2022**, *27*, 3564.
- (10) Shaw, P. E.; Ruseckas, A.; Samuel, I. D. W. Exciton Diffusion Measurements in Poly(3-hexylthiophene). *Adv. Mater.* **2008**, *20*, 3516–3520.
- (11) Yamamoto, H.; Oyamada, T.; Sasabe, H.; Adachi, C. Amplified Spontaneous Emission Under Optical Pumping from an Organic Semiconductor Laser Structure Equipped with Transparent Carrier Injection Electrodes. *Appl. Phys. Lett.* **2004**, *84*, 1401–1403.
- (12) Gartner, C.; Karnutsch, C.; Pfleiderer, C.; Lemmer, U. Numerical Device Simulation of Double-Heterostructure Organic Laser Diodes Including Current-Induced Absorption Processes. *IEEE J. Quantum Elect.* **2007**, *43*, 1006–1017.
- (13) Brown, A.; Pichler, K.; Greenham, N.; Bradley, D.; Friend, R.; Holmes, A. Optical Spectroscopy of Triplet Excitons and Charged Excitations in Poly(p-phenylenevinylene) Light-emitting Diodes. *Chem. Phys. Lett.* **1993**, *210*, 61–66.
- (14) Tautz, R.; Da Como, E.; Limmer, T.; Feldmann, J.; Egelhaaf, H.-J.; von Hauff, E.; Lemaire, V.; Beljonne, D.; Yilmaz, S.; Dumsch, I.; Allard, S.; Scherf, U. Structural Correlations in the Generation of Polaron Pairs in Low Bandgap Polymers for Photovoltaics. *Nat. Commun.* **2012**, *3*, No. 970.
- (15) Tautz, R.; Da Como, E.; Wiebler, C.; Soavi, G.; Dumsch, I.; Fröhlich, N.; Grancini, G.; Allard, S.; Scherf, U.; Cerullo, G.; Schumacher, S.; Feldmann, J. Charge Photogeneration in Donor-Acceptor Conjugated Materials: Influence of Excess Excitation Energy and Chain Length. *J. Am. Chem. Soc.* **2013**, *135*, 4282–4290.
- (16) Christiansen, O.; Koch, H.; Jørgensen, P. The Second-order Approximate Coupled Cluster Singles and Doubles Model CC2. *Chem. Phys. Lett.* **1995**, *243*, 409–418.
- (17) Ågren, H.; Christiansen, O.; Cronstrand, P.; Norman, P. Ab Initio Modeling of Excited State Absorption of Polyenes. *Phys. Chem. Chem. Phys.* **2001**, *3*, 2567–2575.
- (18) Cronstrand, P.; Christiansen, O.; Norman, P.; Ågren, H. Theoretical Calculations of Excited State Absorption. *Phys. Chem. Chem. Phys.* **2000**, *2*, 5357–5363.
- (19) Koch, H.; Jensen, H. J. A.; Jørgensen, P.; Helgaker, T.; Scuseria, G. E.; Schaefer, H. F. Coupled Cluster Energy Derivatives. Analytic Hessian for the Closed-shell Coupled Cluster Singles and Doubles Wave Function: Theory and Applications. *J. Chem. Phys.* **1990**, *92*, 4924–4940.
- (20) Purvis, G. D.; Bartlett, R. J. A Full Coupled-Cluster Singles and Doubles Model: The Inclusion of Disconnected Triples. *J. Chem. Phys.* **1982**, *76*, 1910–1918.
- (21) Fedotov, D. A.; Paul, A. C.; Posocco, P.; Santoro, F.; Garavelli, M.; Koch, H.; Coriani, S.; Improta, R. Excited-State Absorption of Uracil in the Gas Phase: Mapping the Main Decay Paths by Different Electronic Structure Methods. *J. Chem. Theory Comput.* **2021**, *17*, 1638–1652.
- (22) Fedotov, D. A.; Paul, A. C.; Koch, H.; Santoro, F.; Coriani, S.; Improta, R. Excited State Absorption of DNA Bases in the Gas Phase and in Chloroform Solution: a Comparative Quantum Mechanical Study. *Phys. Chem. Chem. Phys.* **2022**, *24*, 4987–5000.
- (23) Roldao, J. C.; Oliveira, E. F.; Milián-Medina, B.; Gierschner, J.; Roca-Sanjuán, D. Accurate Calculation of Excited-State Absorption for Small-to-Medium-Sized Conjugated Oligomers: Multiconfigurational Treatment vs Quadratic Response TD-DFT. *J. Chem. Theory Comput.* **2022**, *18*, 5449–5458.
- (24) Foggi, P.; Neuwahl, F. V. R.; Moroni, L.; Salvi, P. R. $S_1 \rightarrow S_n$ and $S_2 \rightarrow S_n$ Absorption of Azulene: Femtosecond Transient Spectra and Excited State Calculations. *J. Phys. Chem. A* **2003**, *107*, 1689–1696.
- (25) Parker, S. M.; Rappoport, D.; Furche, F. Quadratic Response Properties from TDDFT: Trials and Tribulations. *J. Chem. Theory Comput.* **2018**, *14*, 807–819.
- (26) Fischer, S. A.; Cramer, C. J.; Govind, N. Excited State Absorption from Real-Time Time-Dependent Density Functional Theory. *J. Chem. Theory Comput.* **2015**, *11*, 4294–4303.
- (27) Bowman, D. N.; Asher, J. C.; Fischer, S. A.; Cramer, C. J.; Govind, N. Excited-state Absorption in Tetraphyrin Porphyrins: Comparing Real-time and Quadratic-response Time-Dependent Density Functional Theory. *Phys. Chem. Chem. Phys.* **2017**, *19*, 27452–27462.
- (28) Ling, S.; Schumacher, S.; Galbraith, I.; Paterson, M. J. Excited-State Absorption of Conjugated Polymers in the Near-Infrared and Visible: A Computational Study of Oligofluorenes. *J. Phys. Chem. C* **2013**, *117*, 6889–6895.
- (29) Zhu, H.; Wang, J.; Wang, F.; Feng, E.; Sheng, X. Linear and Quadratic Response TDDFT Methods for the Excited-state Absorption in Oligofluorenes. *Chem. Phys. Lett.* **2021**, *785*, No. 139150.

- (30) Roseli, R. B.; Tapping, P. C.; Kee, T. W. Origin of the Excited-State Absorption Spectrum of Polythiophene. *J. Phys. Chem. Lett.* **2017**, *8*, 2806–2811.
- (31) Sheng, X.; Zhu, H.; Yin, K.; Chen, J.; Wang, J.; Wang, C.; Shao, J.; Chen, F. Excited-State Absorption by Linear Response Time-Dependent Density Functional Theory. *J. Phys. Chem. C* **2020**, *124*, 4693–4700.
- (32) De Wergifosse, M.; Grimme, S. Nonlinear-response Properties in a Simplified Time-dependent Density Functional Theory (sTD-DFT) Framework: Evaluation of Excited-state Absorption Spectra. *J. Chem. Phys.* **2019**, *150*, No. 094112.
- (33) Koch, H.; Christiansen, O.; Jørgensen, P.; Sanchez de Merás, A. M.; Helgaker, T. The CC3Model: An Iterative Coupled Cluster Approach Including Connected Triples. *J. Chem. Phys.* **1997**, *106*, 1808–1818.
- (34) Sarkar, R.; Boggio-Pasqua, M.; Loos, P.-F.; Jacquemin, D. Benchmarking TD-DFT and Wave Function Methods for Oscillator Strengths and Excited-State Dipole Moments. *J. Chem. Theory Comput.* **2021**, *17*, 1117–1132.
- (35) Loos, P.-F.; Scemama, A.; Blondel, A.; Garniron, Y.; Caffarel, M.; Jacquemin, D. A Mountaineering Strategy to Excited States: Highly Accurate Reference Energies and Benchmarks. *J. Chem. Theory Comput.* **2018**, *14*, 4360–4379.
- (36) Schreiber, M.; Silva-Junior, M. R.; Sauer, S. P. A.; Thiel, W. Benchmarks for Electronically Excited States: CASPT2, CC2, CCSD, and CC3. *J. Chem. Phys.* **2008**, *128*, No. 134110.
- (37) Pawłowski, F.; Jørgensen, P.; Hättig, C. Gauge Invariance of Oscillator Strengths in the Approximate Coupled Cluster Triples Model CC3. *Chem. Phys. Lett.* **2004**, *389*, 413–420.
- (38) Pedersen, T. B.; Koch, H. Gauge Invariance of the Coupled Cluster Oscillator Strength. *Chem. Phys. Lett.* **1998**, *293*, 251–260.
- (39) Pedersen, T. B.; Koch, H. Coupled Cluster Response Functions Revisited. *J. Chem. Phys.* **1997**, *106*, 8059–8072.
- (40) Malmqvist, P.; Roos, B. O. The CASSCF State Interaction Method. *Chem. Phys. Lett.* **1989**, *155*, 189–194.
- (41) Stanton, J. F.; Bartlett, R. J. The Equation of Motion Coupled-cluster Cethod. A Systematic Biorthogonal Approach to Molecular Excitation Energies, Transition Probabilities, and Excited State Properties. *J. Chem. Phys.* **1993**, *98*, 7029–7039.
- (42) Paul, A. C.; Myhre, R. H.; Koch, H. New and Efficient Implementation of CC3. *J. Chem. Theory Comput.* **2021**, *17*, 117–126.
- (43) Bartlett, R. J. Coupled-cluster Theory and its Equation-of-motion Extensions. *WIREs Comput. Mol. Sci.* **2012**, *2*, 126–138.
- (44) Koch, H.; Kobayashi, R.; Sanchez De Merás, A.; Jørgensen, P. Calculation of Size-intensive Transition Moments from the Coupled Cluster Singles and Doubles Linear Response function. *J. Chem. Phys.* **1994**, *100*, 4393–4400.
- (45) Caricato, M.; Trucks, G. W.; Frisch, M. J. On the Difference Between the Transition Properties Calculated with Linear Response-and Equation of Motion-CCSD Approaches. *J. Chem. Phys.* **2009**, *131*, No. 174104.
- (46) Schirmer, J. Beyond the Random-phase Approximation: A New Approximation Scheme for the Polarization Propagator. *Phys. Rev. A* **1982**, *26*, 2395–2416.
- (47) Dreuw, A.; Wormit, M. The Algebraic Diagrammatic Construction Scheme for the Polarization Propagator for the Calculation of Excited States. *WIREs Comput. Mol. Sci.* **2015**, *5*, 82–95.
- (48) Norman, P.; Jonsson, D.; Ågren, H. Excited State Properties through Cubic Response Theory: Polarizabilities of Benzene and Naphthalene. *Chem. Phys. Lett.* **1997**, *268*, 337–344.
- (49) Christiansen, O.; Koch, H.; Jørgensen, P. Perturbative Triple Excitation Corrections to Coupled Cluster Singles and Doubles Excitation Energies. *J. Chem. Phys.* **1996**, *105*, 1451–1459.
- (50) Fischer, S. A.; Cramer, C. J.; Govind, N. Excited-State Absorption from Real-Time Time-Dependent Density Functional Theory: Optical Limiting in Zinc Phthalocyanine. *J. Phys. Chem. Lett.* **2016**, *7*, 1387–1391.
- (51) Denis, J.-C.; Ruseckas, A.; Hedley, G. J.; Matheson, A. B.; Paterson, M. J.; Turnbull, G. A.; Samuel, I. D. W.; Galbraith, I. Self-trapping and Excited State Absorption in Fluorene Homo-polymer and Copolymers with Benzothiadiazole and Tri-phenylamine. *Phys. Chem. Chem. Phys.* **2016**, *18*, 21937–21948.
- (52) Han, J.; Rehn, D. R.; Buckup, T.; Dreuw, A. Evaluation of Single-Reference DFT-Based Approaches for the Calculation of Spectroscopic Signatures of Excited States Involved in Singlet Fission. *J. Phys. Chem. A* **2020**, *124*, 8446–8460.
- (53) Jaiswal, V. K.; Segarra-Martí, J.; Marazzi, M.; Zvereva, E.; Assfeld, X.; Monari, A.; Garavelli, M.; Rivalta, I. First-principles Characterization of the Singlet Excited State Manifold in DNA/RNA Nucleobases. *Phys. Chem. Chem. Phys.* **2020**, *22*, 15496–15508.
- (54) Vérit, M.; Scemama, A.; Caffarel, M.; Lipparini, F.; Boggio-Pasqua, M.; Jacquemin, D.; Loos, P.-F. QUESTDB: A Database of Highly Accurate Excitation Energies for the Electronic Structure Community. *WIREs Comput. Mol. Sci.* **2021**, *11*, e1517.
- (55) Abreha, B. G.; Agarwal, S.; Foster, I.; Blaiszik, B.; Lopez, S. A. Virtual Excited State Reference for the Discovery of Electronic Materials Database: An Open-Access Resource for Ground and Excited State Properties of Organic Molecules. *J. Phys. Chem. Lett.* **2019**, *10*, 6835–6841.
- (56) Becke, A. D. Density-Functional Thermochemistry. III. The Role of Exact Exchange. *J. Chem. Phys.* **1993**, *98*, 5648–5652.
- (57) Lee, C.; Yang, W.; Parr, R. G. Development of the Colle-Salvetti Correlation-Energy Formula into a Functional of the Electron Density. *Phys. Rev. B* **1988**, *37*, 785–789.
- (58) Stephens, P. J.; Devlin, F. J.; Chabalowski, C. F.; Frisch, M. J. Ab Initio Calculation of Vibrational Absorption and Circular Dichroism Spectra Using Density Functional Force Fields. *J. Phys. Chem. A* **1994**, *98*, 11623–11627.
- (59) Vosko, S. H.; Wilk, L.; Nusair, M. Accurate Spin-Dependent Electron Liquid Correlation Energies for Local Spin Density Calculations: a Critical Analysis. *Can. J. Phys.* **1980**, *58*, 1200–1211.
- (60) Becke, A. D. A New Mixing of Hartreefock and Local Density-functional Theories. *J. Chem. Phys.* **1993**, *98*, 1372–1377.
- (61) Yanai, T.; Tew, D. P.; Handy, N. C. A New Hybrid Exchange-Correlation Functional Using the Coulomb-Attenuating Method (CAM-B3LYP). *Chem. Phys. Lett.* **2004**, *393*, 51–57.
- (62) Ikura, H.; Tsuneda, T.; Yanai, T.; Hirao, K. A Long-Range Correction Scheme for Generalized-Gradient-Approximation Exchange Functionals. *J. Chem. Phys.* **2001**, *115*, 3540–3544.
- (63) Loos, P.-F.; Jacquemin, D. Chemically Accurate 0–0 Energies with not-so-Accurate Excited State Geometries. *J. Chem. Theory Comput.* **2019**, *15*, 2481–2491.
- (64) Dalton, A. Molecular Electronic Structure Program, 2020, <http://daltonprogram.org> (last accessed: December 19, 2024).
- (65) Aidas, K.; Angeli, C.; Bak, K. L.; Bakken, V.; Bast, R.; Boman, L.; Christiansen, O.; Cimiraglia, R.; Coriani, S.; Dahle, P.; Dalskov, E. K.; Ekström, U.; Enevoldsen, T.; Eriksen, J. J.; Ettenhuber, P.; Fernández, B.; Ferrighi, L.; Fliegl, H.; Frediani, L.; Hald, K.; Halkier, A.; Hättig, C.; Heiberg, H.; Helgaker, T.; Hennum, A. C.; Hettema, H.; Hjertenæs, E.; Høst, S.; Høyvik, I.-M.; Iozzi, M. F.; Jansik, B.; Jensen, H. J. Aa.; Jonsson, D.; Jørgensen, P.; Kauczor, J.; Kirpekar, S.; Kjærgaard, T.; Klopper, W.; Knecht, S.; Kobayashi, R.; Koch, H.; Kongsted, J.; Krapp, A.; Kristensen, K.; Ligabue, A.; Lutnæs, O. B.; Melo, J. I.; Mikkelsen, K. V.; Myhre, R. H.; Neiss, C.; Nielsen, C. B.; Norman, P.; Olsen, J.; Olsen, J. M. H.; Østed, A.; Packer, M. J.; Pawłowski, F.; Pedersen, T. B.; Provasi, P. F.; Reine, S.; Rinkevicius, Z.; Ruden, T. A.; Ruud, K.; Rybkin, V. V.; Salek, P.; Samson, C. C. M.; de Merás, A. S.; Sauve, T.; Sauer, S. P. A.; Schimelpfennig, B.; Snæskov, K.; Steindal, A. H.; Sylvester-Hvid, K. O.; Taylor, P. R.; Teale, A. M.; Tellgren, E. I.; Tew, D. P.; Thorvaldsen, A. J.; Thøgersen, L.; Vahtras, O.; Watson, M. A.; Wilson, D. J. D.; Ziolkowski, M.; Ågren, H. The Dalton Quantum Chemistry Program System. *WIREs Comput. Mol. Sci.* **2014**, *4*, 269–284.
- (66) Pecul, M.; Pawłowski, F.; Jørgensen, P.; Köhn, A.; Hättig, C. High-Order Correlation Effects on Dynamic Hyperpolarizabilities and

- their Geometric Derivatives: A Comparison with Density Functional Results. *J. Chem. Phys.* **2006**, *124*, No. 114101.
- (67) Hättig, C.; Christiansen, O.; Koch, H.; Jørgensen, P. Frequency-Dependent First Hyperpolarizabilities Using Cluster Quadratic Response Theory. *Chem. Phys. Lett.* **1997**, *269*, 428–434.
- (68) Schirmer, J.; Trofimov, A. B. Intermediate State Representation Approach to Physical Properties of Electronically Excited Molecules. *J. Chem. Phys.* **2004**, *120*, 11449–11464.
- (69) Epifanovsky, E.; Gilbert, A. T. B.; Feng, X.; Lee, J.; Mao, Y.; Mardirossian, N.; Pokhilko, P.; White, A. F.; Coons, M. P.; Dempwolff, A. L.; Gan, Z.; Hait, D.; Horn, P. R.; Jacobson, L. D.; Kaliman, I.; Kussmann, J.; Lange, A. W.; Lao, K. U.; Levine, D. S.; Liu, J.; McKenzie, S. C.; Morrison, A. F.; Nanda, K. D.; Plasser, F.; Rehn, D. R.; Vidal, M. L.; You, Z.-Q.; Zhu, Y.; Alam, B.; Albrecht, B. J.; Aldossary, A.; Alguire, E.; Andersen, J. H.; Athavale, V.; Barton, D.; Begam, K.; Behn, A.; Bellonzi, N.; Bernard, Y. A.; Berquist, E. J.; Burton, H. G. A.; Carreras, A.; Carter-Fenk, K.; Chakraborty, R.; Chien, A. D.; Closser, K. D.; Cofer-Shabica, V.; Dasgupta, S.; de Wergifosse, M.; Deng, J.; Diedenhofen, M.; Do, H.; Ehler, S.; Fang, P.-T.; Fatehi, S.; Feng, Q.; Friedhoff, T.; Gayvert, J.; Ge, Q.; Gidofalvi, G.; Goldey, M.; Gomes, J.; González-Espinoza, C. E.; Gulania, S.; Gunina, A. O.; Hanson-Heine, M. W. D.; Harbach, P. H. P.; Hauser, A.; Herbst, M. F.; Hernández Vera, M.; Hodecker, M.; Holden, Z. C.; Houck, S.; Huang, X.; Hui, K.; Huynh, B. C.; Ivanov, M.; Jász, A.; Ji, H.; Jiang, H.; Kaduk, B.; Kähler, S.; Khistyaev, K.; Kim, J.; Kis, G.; Klunzinger, P.; Koczor-Benda, Z.; Koh, J. H.; Kosenkov, D.; Koulias, L.; Kowalczyk, T.; Krauter, C. M.; Kue, K.; Kunitsa, A.; Kus, T.; Ladjánszki, I.; Landau, A.; Lawler, K. V.; Lefrancois, D.; Lehtola, S.; Li, R. R.; Li, Y.-P.; Liang, J.; Liebenthal, M.; Lin, H.-H.; Lin, Y.-S.; Liu, F.; Liu, K.-Y.; Loipersberger, M.; Luenser, A.; Manjanath, A.; Manohar, P.; Mansoor, E.; Manzer, S. F.; Mao, S.-P.; Marenich, A. V.; Markovich, T.; Mason, S.; Maurer, S. A.; McLaughlin, P. F.; Menger, M. F. S. J.; Mewes, J.-M.; Mewes, S. A.; Morgante, P.; Mullinax, J. W.; Oosterbaan, K. J.; Paran, G.; Paul, A. C.; Paul, S. K.; Pavošević, F.; Pei, Z.; Prager, S.; Proynov, E. I.; Rák, A.; Ramos-Cordoba, E.; Rana, B.; Rask, A. E.; Rettig, A.; Richard, R. M.; Rob, F.; Rossomme, E.; Scheele, T.; Scheurer, M.; Schneider, M.; Sergueev, N.; Sharada, S. M.; Skomorowski, W.; Small, D. W.; Stein, C. J.; Su, Y.-C.; Sundstrom, E. J.; Tao, Z.; Thirman, J.; Tornai, G. J.; Tsuchimochi, T.; Tubman, N. M.; Veccham, S. P.; Vydrov, O.; Wenzel, J.; Witte, J.; Yamada, A.; Yao, K.; Yeganeh, S.; Yost, S. R.; Zech, A.; Zhang, I. Y.; Zhang, X.; Zhang, Y.; Zuev, D.; Aspuru-Guzik, A.; Bell, A. T.; Besley, N. A.; Bravaya, K. B.; Brooks, B. R.; Casanova, D.; Chai, J.-D.; Coriani, S.; Cramer, C. J.; Cserey, G.; DePrince, I.; Eugene, A.; DiStasio, J.; Robert, A.; Dreuw, A.; Dunietz, B. D.; Furlani, T. R.; Goddard, I.; William, A.; Hammes-Schiffer, S.; Head-Gordon, T.; Hehre, W. J.; Hsu, C.-P.; Jagau, T.-C.; Jung, Y.; Klamt, A.; Kong, J.; Lambrecht, D. S.; Liang, W.; Mayhall, N. J.; McCurdy, C. W.; Neaton, J. B.; Ochsenfeld, C.; Parkhill, J. A.; Peverati, R.; Rassolov, V. A.; Shao, Y.; Slipchenko, L. V.; Stauch, T.; Steele, R. P.; Subotnik, J. E.; Thom, A. J. W.; Tkatchenko, A.; Truhlar, D. G.; Van Voorhis, T.; Wesolowski, T. A.; Whaley, K. B.; Woodcock, I.; Lee, H.; Zimmerman, P. M.; Faraji, S.; Gill, P. M. W.; Head-Gordon, M.; Herbert, J. M.; Krylov, A. I. Software for the Frontiers of Quantum Chemistry: An Overview of Developments in the Q-chem 5 Package. *J. Chem. Phys.* **2021**, *155*, No. 084801.
- (70) Jorgensen, P.; Jensen, H. J. A.; Olsen, J. Linear Response Calculations for Large Scale Multiconfiguration Self-Consistent Field Wave Functions. *J. Chem. Phys.* **1988**, *89*, 3654–3661.
- (71) Vahtras, O.; Ågren, H.; Jørgensen, P.; Jensen, H. J. A.; Helgaker, T.; Olsen, J. Multiconfigurational Quadratic Response Functions for Singlet and Triplet Perturbations: The Phosphorescence Lifetime of Formaldehyde. *J. Chem. Phys.* **1992**, *97*, 9178–9187.
- (72) Ågren, H.; Vahtras, O.; Koch, H.; Jørgensen, P.; Helgaker, T. Direct Atomic Orbital Based Self-Consistent-Field Calculations of Nonlinear Molecular Properties. Application to the Frequency Dependent Hyperpolarizability of *Para*-nitroaniline. *J. Chem. Phys.* **1993**, *98*, 6417–6423.
- (73) Garniron, Y.; Applencourt, T.; Gasperich, K.; Benali, A.; Ferté, A.; Paquier, J.; Pradines, B.; Assaraf, R.; Reinhardt, P.; Toulouse, J.; Barbaresco, P.; Renon, N.; David, G.; Malrieu, J.-P.; Vérit, M.; Caffarel, M.; Loos, P.-F.; Giner, E.; Scemama, A. Quantum Package 2.0: An Open-Source Determinant-Driven Suite of Programs. *J. Chem. Theory Comput.* **2019**, *15*, 3591–3609.
- (74) Damour, Y.; Scemama, A.; Kossoски, F.; Loos, P.-F. Selected Configuration Interaction for Resonances. *J. Phys. Chem. Lett.* **2024**, *15*, 8296–8305.
- (75) Damour, Y.; Quintero-Monsebaiz, R.; Caffarel, M.; Jacquemin, D.; Kossoски, F.; Scemama, A.; Loos, P.-F. Ground- and Excited-State Dipole Moments and Oscillator Strengths of Full Configuration Interaction Quality. *J. Chem. Theory Comput.* **2023**, *19*, 221–234.
- (76) Naim, C.; Zalešny, R.; Jacquemin, D. Two-Photon Absorption Strengths of Small Molecules: Reference CC3 Values and Benchmarks. *J. Chem. Theory Comput.* **2024**, *20*, 9093–9106.
- (77) Tozer, D. J.; Handy, N. C. Improving Virtual Kohn-Sham Orbitals and Eigenvalues: Application to Excitation Energies and Static Polarizabilities. *J. Chem. Phys.* **1998**, *109*, 10180–10189.
- (78) Casida, M. E.; Jamorski, C.; Casida, K. C.; Salahub, D. R. Molecular Excitation Energies to High-Lying Bound States from Time-Dependent Density-Functional Response Theory: Characterization and Correction of the Time-Dependent Local Density Approximation Ionization Threshold. *J. Chem. Phys.* **1998**, *108*, 4439–4449.
- (79) Liang, J.; Feng, X.; Hait, D.; Head-Gordon, M. Revisiting the Performance of Time-Dependent Density Functional Theory for Electronic Excitations: Assessment of 43 Popular and Recently Developed Functionals from Rungs One to Four. *J. Chem. Theory Comput.* **2022**, *18*, 3460–3473.